Investigations into the Feasibility of Optical-CT 3D Dosimetry with Minimal Use of Refractively Matched Fluids

by

Kelsey Leigh Chisholm

Graduate Program in Medical Physics
Duke University

Date:_____

Approved:

_____
Mark Oldham, Supervisor

_____
Justus Adamson

_____
Joseph Lo

Thesis submitted in partial fulfillment of
the requirements for the degree of
Master of Science in the Department of
Medical Physics in the Graduate School
of Duke University

2014

ABSTRACT

Investigations into the Feasibility of Optical-CT 3D Dosimetry with Minimal Use of Refractively Matched Fluids

by

Kelsey Leigh Chisholm

Graduate Program in Medical Physics
Duke University

Date:_____

Approved:

_____
Mark Oldham, Supervisor

_____
Justus Adamson

_____
Joseph Lo

An abstract of a thesis submitted in partial fulfillment of the requirements for the degree of Master of Science in the Department of Medical Physics in the Graduate School of Duke University

2014

Abstract

Purpose: Optical-CT imaging with radiochromic dosimeters is a powerful method of evaluating 3D dose distributions at high resolution and sensitivity. Current optical-CT systems require large quantities of refractively matched fluid surrounding the dosimeter in order to minimize refraction artifacts. The use of a refractively matched solid polyurethane solid-tank, in place of a fluid bath, has the potential to greatly increase practical convenience, reduce cost, and improve the efficacy of flood corrections. This thesis aims to investigate the feasibility of solid-tank optical-CT imaging for 3D dosimetry, and to use computer simulation to investigate optimal design and scanning parameters.

Methods: A Matlab based ray-tracing simulation platform, ScanSim, was used to model a parallel-source imaging system through a cubic polyurethane solid-tank containing a central cylindrical hollow into which cylindrical PRESAGE® radiochromic dosimeters can be placed. A small amount of fluid surrounds the dosimeter in the tank. ScanSim's capabilities were expanded from previous work to include the geometry and physics of dry scanning. Two imaging methods were investigated, representing a telecentric detector and an ideal detector: in the latter, all light rays are collected and used in reconstruction. In order to characterize the efficacy of these systems, and dependence on refractive index (RI) mismatches between dosimeter, solid-tank, and fluid,

simulations were run for a variety of dosimeter (RI = 1.5-1.47), and fluid (RI = 1.55-1.0) combinations. Additional simulations examined the effect of increasing gap size (1-5mm) between the dosimeter and solid-tank well. For the telecentric setup, the effects of changing the lens tolerance (0.5-5.0 degrees) were also investigated. The metric for evaluation of efficacy is the *usable radius*, which is defined as the distance from the dosimeter center where the measured and true (known) dose differs by less than 2%. Results: As the refractive index mismatch between the dosimeter and tank increases from 0-0.02, the telecentric system showed a significant decrease in the usable radius from 97.6% to 50.2% compared to a decrease from 97.6% to 96.4% for the ideal system. When the three media are perfectly matched, the telecentric system and ideal system perform identically. For mismatched dosimeter and solid-tank in a telecentric system, the optimal fluid match has a refractive index lower than either the tank or dosimeter, decreasing non-linearly from 1.5-1.34 as the dosimeter-tank refractive mismatch increases from 0 to 0.02. Media mismatches between the dosimeter and solid-tank also exacerbate the effects of changing the gap size, with no apparent quantifiable relationship. Generally, the optimal fluid match is closer to the dosimeter RI when the gap size is large (>3mm). Increasing the telecentric lens tolerance improves the usable radius for all refractive media combinations, and approaches the behavior of the ideal system for tolerances >5.0°.

Conclusions: Results show dry optical-CT imaging in a telecentric system is feasible if the dosimeter RI is a close match with the solid-tank (<0.01 difference), providing accurate dose measurements within ±2% of true dose to over 80% of the dosimeter volume. In order to achieve accurate measurements over 96% of the dosimeter volume (representing out to 2mm from the dosimeter edge), the dosimeter-tank RI mismatch must be less than 0.005. However, large RI mismatches lead to dose discrepancies outside the central volume of the dosimeter, so this system is feasible for these situations only if data in the periphery is not required. The ScanSim tool proved very useful in situations when the tank and dosimeter had slight differences in RI by enabling estimation of the optimal choice of RI of the small amount of surrounding fluid still required for dry scanning, albeit by a trial-and-error process. For mismatched dosimeter and tank RI, the optimal fluid RI choice is lower than the dosimeter, though the amount lower depends on both the magnitude of dosimeter-tank RI mismatch and the gap size. Some spoiling of the telecentric beam and increasing the telecentric lens tolerance to greater than 1.0° helps recover the usable radius in situations with media mismatches, potentially increasing the range of feasible media combinations.

Dedication

To my fiancé, Michael, and my family.

Contents

List of Tables

List of Figures

Acknowledgements

I would like to acknowledge my advisor, Dr. Mark Oldham, for his invaluable advice and support. I also want to extend a special thanks to Leith Rankine for teaching me ScanSim and meticulously commenting his code so I could build upon it. Finally, I would like to thank my committee members Dr. Justus Adamson and Dr. Joseph Lo for their time, effort, and feedback.

1. Introduction

1.1 Optical-CT Imaging with 3D Radiochromic Dosimeters

Optical computed tomography is a technique in which visible wavelength light is used to image radiation dose distributions in materials whose optical density is affected by exposure to ionizing radiation. Since Gore *et al* introduced the first optical-CT system to image polymer-gel dosimeters in 1996[6], optical-CT has gained traction as a robust, precise, and clinically-effective method of evaluating dose distributions in a 3D dosimeter[7, 19, 21]. Optical-CT uses the same physics principles as regular x-ray CT (Beer's Law, Radon transforms, and reconstruction with filtered backprojection), but uses a visible light source instead of an x-ray source[3, 5]. Various types of optical-CT systems have been developed and evaluated since the technique's inception, and each has merits and limitations.

First-generation laser scanners like that employed by Gore *et al* were eventually developed and marketed by MGS Research, Inc as OCTOPUS™ scanners. These single-beam systems tended to produce high quality images, and for a long time were the only commercially available optical-CT scanners on the market[4, 12]. While these systems have, in the past, been referred to as the "gold standard"[18] for optical-CT, a major disadvantage is their slow scanning speed. Early models took as long as 12 minutes per slice[9], and scan times today with translating single-beam laser readout still require nearly 16 hours for a full 3D scan[4]. Scanners based on charge-coupled device (CCD) area

detectors exist in parallel-beam and cone-beam configurations, and use broad beam light sources to obtain 2D projections rather than acquiring data slice-by-slice[4]. While scanning times tend to be faster, these systems are more susceptible to refraction artifacts[3, 5]. Recent developments in "fast laser scanners" utilizing rotating mirror or other technologies promise to combine the advantages of single-beam laser scanners with the speed of CCD scanners[2, 4, 11]. This work will focus on parallel-beam configurations common to those developed in-house at Duke.

1.1.1 Telecentric Systems

A key component of parallel-beam design for optical-CT scanner is the use of telecentric optics. One of the primary challenges of broad beam optical-CT is that the light rays do not travel in straight lines through the sample due to refraction, invalidating the very principles of image reconstruction for CT[4]. Parallel-beam systems like the Duke large-field-of-view optical-CT scanner (DLOS), developed in-house, make use of a matched telecentric source and imaging lens to project a parallel beam through the dosimeter to the imaging lens, creating an ideal design for parallel beam CT geometry[20].

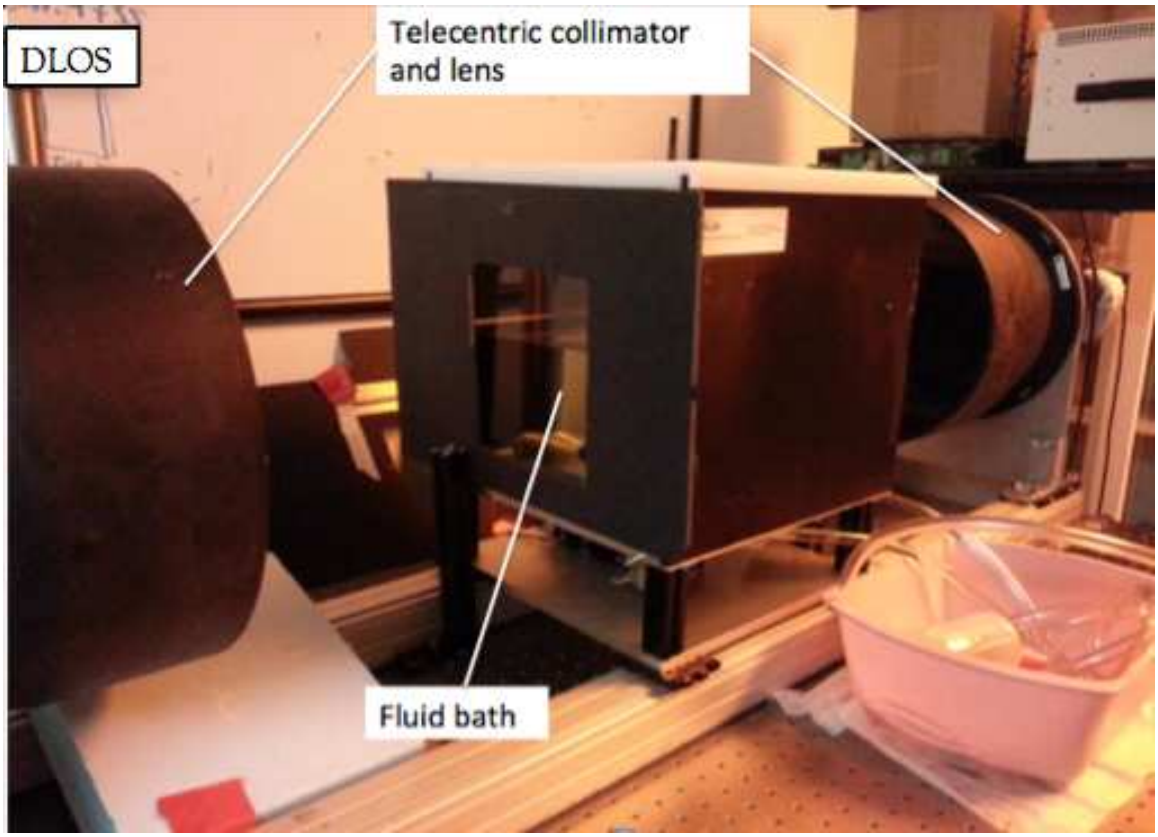

Figure 1: Duke large-field-of-view optical-CT scanner (DLOS)[20], consisting of fluid tank, telecentric collimator and detector, and turntable.

Telecentric lenses have acceptance criteria where light incident on the detector with an angle greater than the criterion will not be detected. This property ensures that image formation is primarily by rays that traverse paths parallel to the optical axis, reducing artifacts from scattered or stray light sources and increasing the accuracy of projection images[18]. Telecentric lenses have the additional benefit that image magnification is independent of the object's position or distance in the field of view.

1.1.2 PRESAGE® and Other Optical-CT Dosimeters

Initial work with optical-CT involved the use of gel dosimetry with Fricke gel or polymer gel. Fricke, or ferrous xylenol-orange (FXG) gel, is highly reproducible and easy to manufacture, but suffers from diffusion of dose patterns post-irradiation[4, 8]. Polymer gels are stable and highly sensitive, but are sensitive to oxygen and attenuate light through scattering, making them susceptible to artifacts[4, 8, 12]. New solid dosimeters like PRESAGE® have a number of potential advantages over gel dosimeters, including insensitivity to oxygen, attenuation due to light absorption rather than scatter, and a rigid structure that is easily machined into a required shape or size[4, 8]. PRESAGE® dosimeters are composed of a polyurethane matrix doped with radiochromic leuco dyes that change color when exposed to ionizing radiation[1, 8]. PRESAGE® exhibits a reproducible, stable dose response, good post-irradiation storage properties, and is considered to be a robust and clinically relevant 3D dosimeter for optical-CT[8, 19, 20]. Current in-house systems make use of parallel-beam configurations with telecentric lenses to image PRESAGE® dosimeters.

1.1.3 Limitations of Current System

Optical-CT scanning has long relied on immersion of samples in refractively matched fluid baths to mitigate refraction artifacts. Refractive index (RI) matching is a time-consuming trial-and-error process of mixing two liquids whose RIs bracket the sample RI that can take up to several hours when large quantities of fluid are required[5]. These high RI fluids tend to be very viscous, rendering them susceptible to thermal

convection currents and 'swirls' of altered RI that mandate a wait period between mixing and scanning to allow the sample to settle. This waiting period is also used to allow any dust motes or airborne particulates that may have accumulated in the fluid to settle so they won't be seen in the projections and cause artifacts in the final image[5, 17]. High viscosity also presents problems during scans, since fast sample rotation will cause vortices and other motion artifacts[5]. All of these factors severely limit the throughput of current optical-CT systems like DLOS, and open the door for novel scanner design that could eliminate many of these factors.

1.2 Purpose and Scope: An Investigation of 'Dry' Scanning

Dry scanning (or "free space scanning") systems generally seek accurate optical-CT scanning in air rather than refractively matched fluid. Several types of dry scanners have been proposed and evaluated before[11, 13, 15], but results showed significant imaging artifacts or large dose discrepancies outside of a small central volume of the dosimeter[5, 14, 16]. In light of these results, we propose a third type of optical-CT system that could potentially overcome the limitations of fluid-based systems and produce more encouraging results than free space scanning systems. The purpose of this thesis is to explore the feasibility of optical-CT with a novel solid-tank telecentric system, and to determine the optimal design and scanning parameters of that system. For the system explored in this work, "dry scanning" is a slight misnomer, as scanning still requires small amounts (~10mL) of refractively matched fluid between the solid-tank walls and

the dosimeter. Even so, this represents a significant improvement over the several liters of fluid required for the current system, so the appellation seems appropriate. The scanner evaluated in this work is analogous in setup to the current in-house system, DLOS, but the fluid bath is replaced with a molded polyurethane block called a "solid-tank". The solid-tank has a central cylindrical well to hold the dosimeter and turntable, and has similar dimensions to the replaced fluid bath. A photograph of the setup is shown in Figure (2). Imaging is done with telecentric lenses and collimators, and scanning procedures are the same.

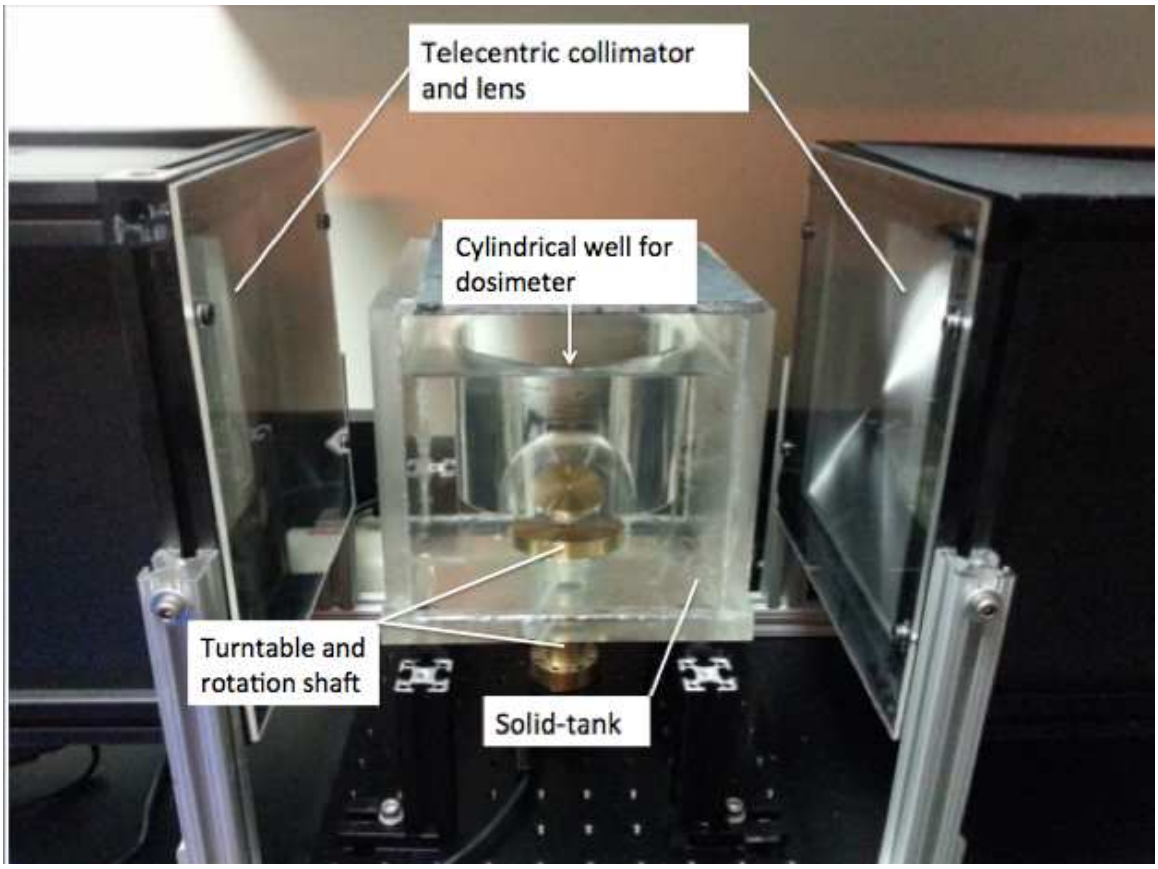

Figure 2: Duke Fresnel-based optical-CT scanner (DFOS), consisting of a solid

polyurethane tank, telecentric collimator and detector, turntable, and central cylindrical well for dosimeter

1.2.1 Potential Benefits of Dry Scanning

A dry scanner offers some significant benefits over traditional fluid bath setups, both in practical convenience and cost. Because the solid-tank has a similar refractive index to PRESAGE® dosimeters, refraction artifacts are minimized without requiring large quantities of refractively matched fluid. In addition to cost saving, this makes a dry scanning system much easier to use and maintain by mitigating the limitations of the use of high RI fluids. In terms of image quality, imperfections in the tank can be almost completely eliminated by taking a pre-scan flood image and subtracting it from the post-scan image. An example is shown in Figure (3) and Figure (4).

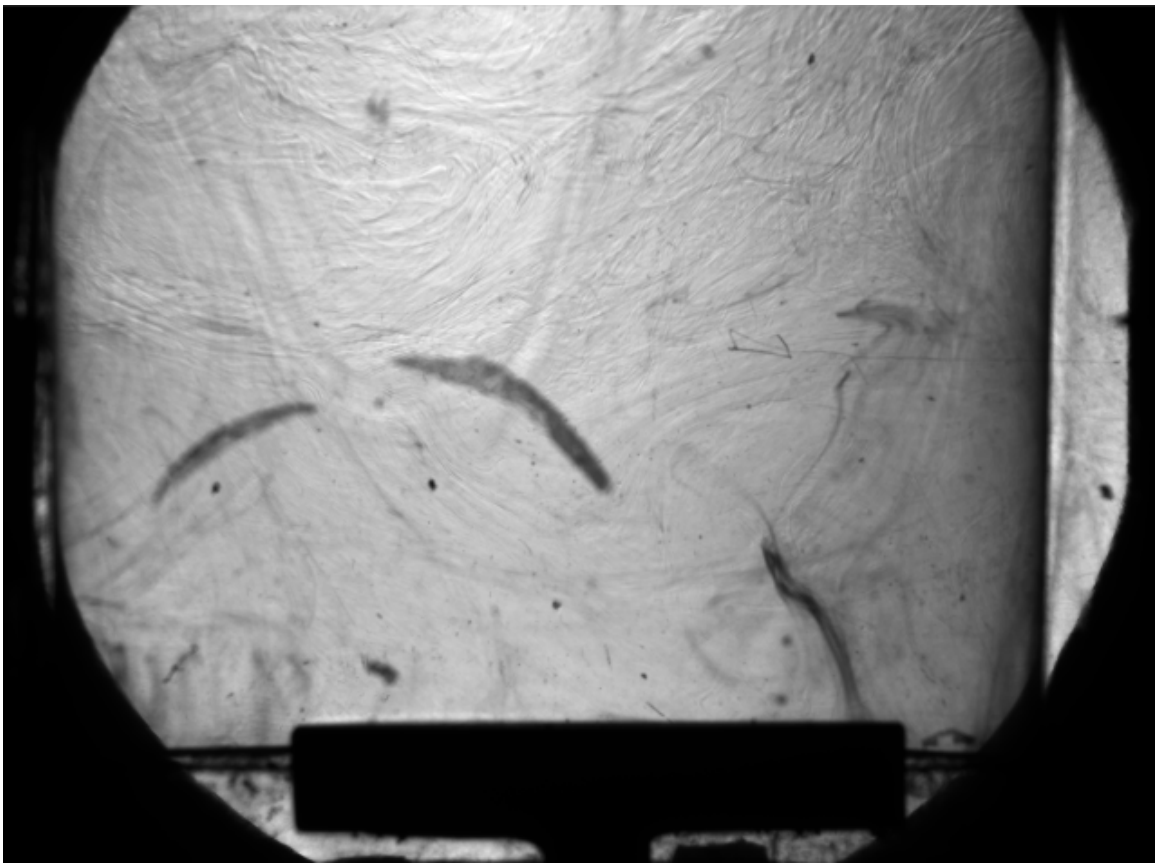

Figure 3: Flood image through a first prototype solid-tank when filled with RI matching fluid. Prominent defects and Schlieren bands are visible. These stationary defects are eliminated from the final image by dividing out the flood image during reconstruction (flood corrected image shown in Figure 4).

Figure 4: Post-scan image of dosimeter taken with a first prototype solid-tank. This dosimeter had received a prior brachytherapy irradiation in the central channel, then a secondary orthogonal beam irradiation. After dividing out the flood image shown in Figure (3), this post-scan image is clean, without evidence of the defects or Schlieren bands.

1.3 Simulation

This thesis involves an extension of previous work done with ScanSim, a Matlab-based ray-tracing program previously used to simulate 3D dosimetry with optical-CT in fluid baths. In ScanSim, ray tracing records the path inside the dosimeter and surrounding media, the relative intensity loss due to transmission losses at boundaries, and attenuation based on optical density[13, 17]. This gives us a powerful tool to manipulate scanning parameters and evaluate their influence without spending time and resources on repeated scans. We can also use ScanSim to estimate the optimal

choice of refractive index of the small amount of fluid still required in dry scanning. The scope of this thesis is to use ScanSim to investigate the achievable accuracy of dry optical-CT 3D dosimetry for the various combinations of refractive media, detector type, and solid-tank geometry.

2. Materials and Methods

Due to the novelty of dry scanning systems for optical-CT and the number of variables involved, the most efficient and accurate way to explore its properties is to simulate common scanning scenarios.

2.1 ScanSim

ScanSim is a GUI-based Matlab program designed to simulate optical-CT of cylindrical dosimeters with a range of useful customizations. An image is shown in Figure (5) below.

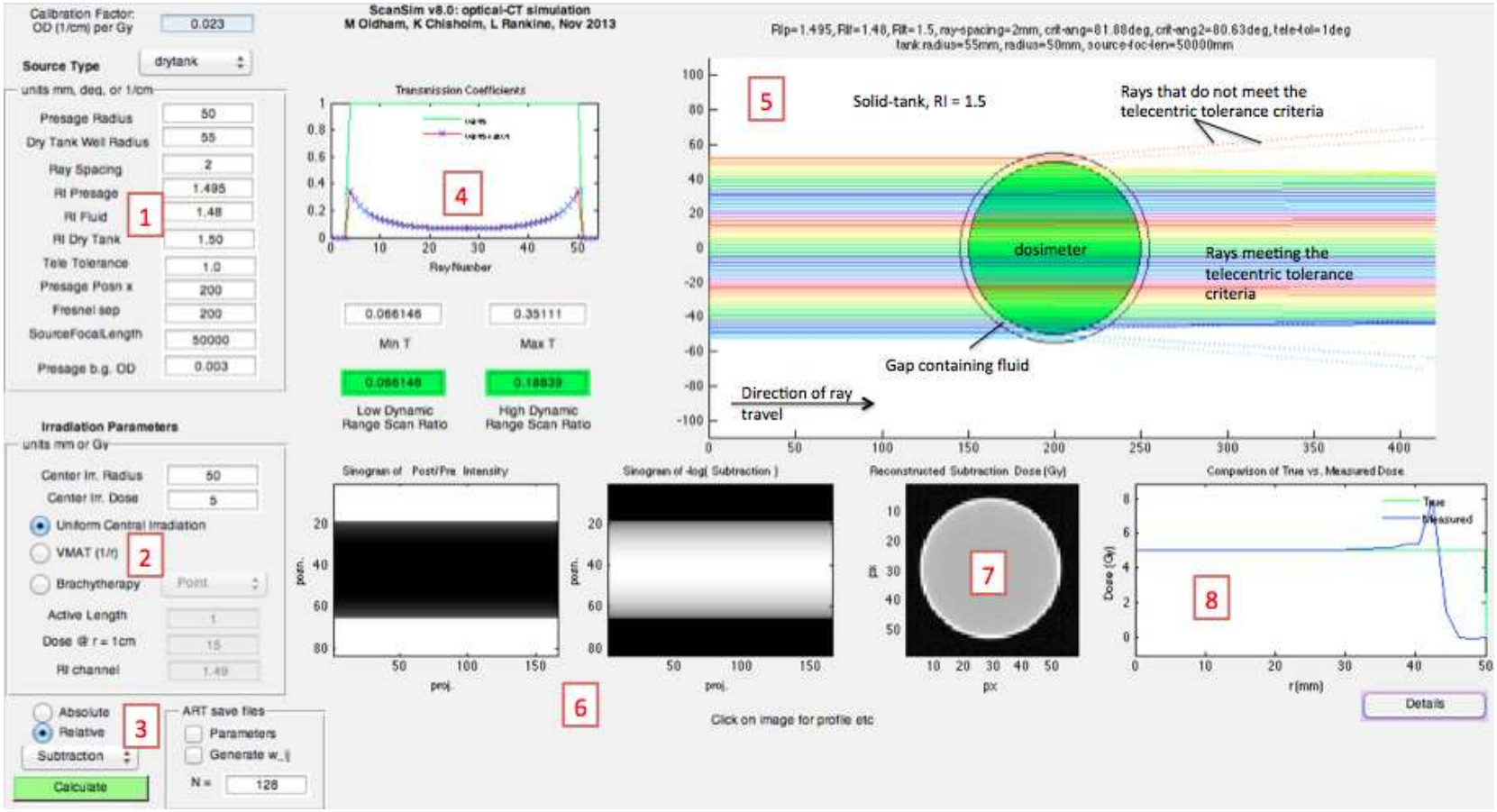

Figure 5: the ScanSim GUI includes inputs for physical parameters (1), irradiation parameters (2), and reconstruction parameters (3). Outputs include transmission factors (4), ray tracing (5), sinograms (6), reconstructed subtracted dose image (7), and comparison of true and measured dose measured radially out from the center of the dosimeter, used for determination of the usable radius (8). Ray colors are artificial and facilitate discerning different ray paths.

The user has inputs for physical parameters such as ray spacing, dosimeter and solid-tank well size, the refractive indices of each media, the telecentric lens tolerance, positioning, and other lens specifications. Inputs for irradiation parameters include the dose distribution (uniform central irradiation, VMAT, or brachytherapy), as well as the dose and the volume to irradiate. Users can choose absolute or relative reconstruction using the default filtered backprojection (FBP) or an algebraic reconstruction technique (ART).

ScanSim outputs a variety of information for each simulation. The transmission coefficients are displayed for each ray along with minimum and maximum transmission factors and the high and low dynamic range scan ratio. The main visual output, as shown in Figure (6), is a top-down view of the ray-tracings through the specified geometry, including an indication of which rays meet the telecentric criteria. Solid rays represent those whose angle of incidence is less than or equal to the telecentric tolerance, and dotted rays represent those scattered outside of the telecentric tolerance window.

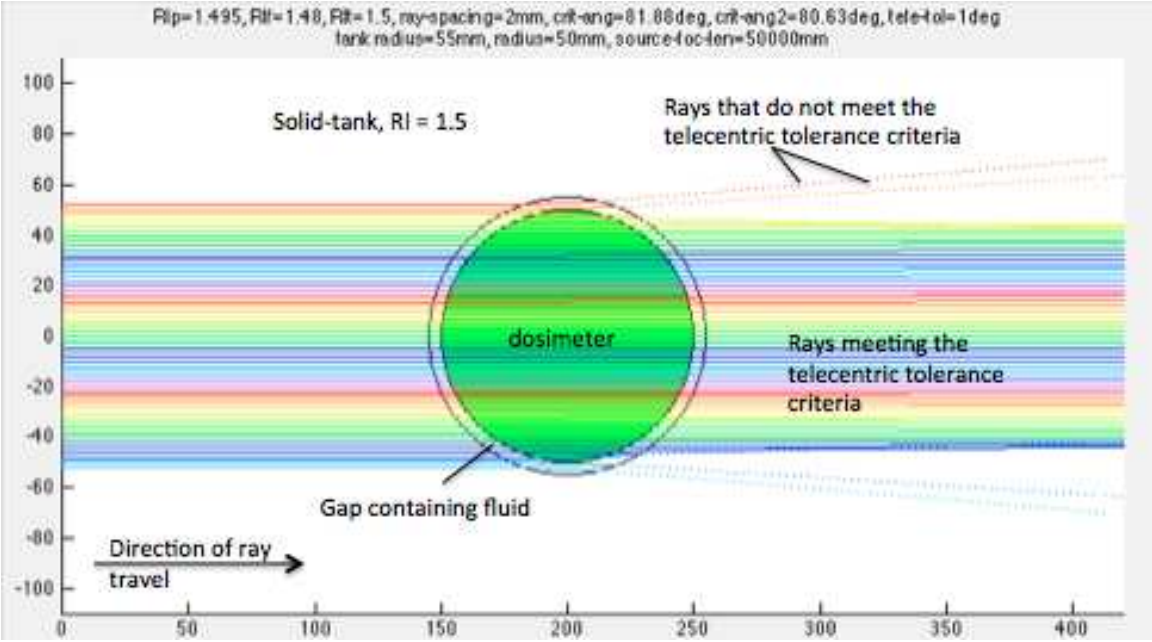

Figure 6: Ray tracing in ScanSim. Ray colors are artificial and serve to facilitate discerning different ray paths. In this example, dosimeter RI = 1.495, solid-tank RI = 1.5, and fluid RI = 1.48.

The recorded intensity, angle, and distance from the center for each ray are displayed in sinograms for projections over 360°, along with a reconstructed subtraction dose image[13, 17]. Finally, the GUI has a graphical display of true vs. measured dose within the dosimeter. Each output image can be expanded for access to various analysis tools.

2.1.1 Physics Principles Involved

There are several fundamental physics principles involved in the ray-tracing process, as described in earlier works[13, 17]. A graphical representation of these principles and variables is shown in Figure (7).

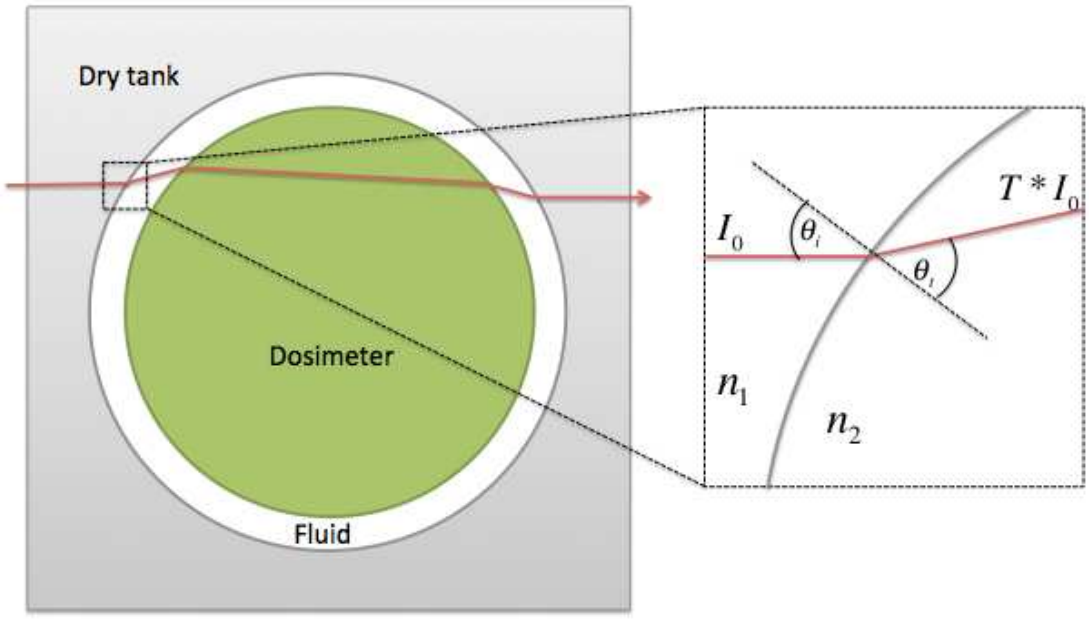

Figure 7: Physics properties of ScanSim. A light ray incident on a media boundary experiences refraction and transmission losses according to Eq. (1) and Eq. (4), respectively. In this diagram, $n_1 > n_{dosimeter} > n_2$**.**

The simulation obeys the laws of refraction as dictated by Snell's Law (1); a light ray incident on a refractively mismatched media boundary ($n_1 \rightarrow n_2$) at angle θ_i will be refracted and exit the boundary with angle θ_t:

$$\theta_t = \arcsin\left(\frac{n_1 \sin\theta_i}{n_2}\right) \tag{1}$$

As the ray traverses the boundary, it will suffer transmission losses from partial transmission and reflection in accordance with the Fresnel equations. For unpolarized light, the fraction of transmitted intensity T is given by equation (4).

$$R_s = \left| \frac{n_1 \sin\theta_i - n_2 \sin\theta_t}{n_1 \sin\theta_i + n_2 \sin\theta_t} \right|^2 \tag{2}$$

$$R_p = \left| \frac{n_1 \sin\theta_t - n_2 \sin\theta_i}{n_1 \sin\theta_t + n_2 \sin\theta_i} \right|^2 \tag{3}$$

$$T = 1 - \frac{R_s + R_p}{2} \tag{4}$$

The path length in the irradiated medium also affects the intensity of light rays. The radiochromic response of PRESAGE® means the OD of the dosimeter increases in irradiated sections. The attenuation is found from Eq. (5), and solved analytically for uniform dose distributions:

$$\log_{10}\left(\frac{I}{I_0}\right) = \int_{s_1}^{s_2} OD(r) \cdot ds \tag{5}$$

2.1.2 ScanSim Methodology

ScanSim models rays based on the specified ray spacing, physical properties, and simulated dose distribution, OD(*r*). Information about the ray path, intensity, and angle are recorded for each stage of the simulation and recorded in a sinogram. The pre- and post-scan intensity values are converted to OD, transmission loss effects are removed by subtraction, and then reconstructed using filtered backprojection. Because this requires a full set of evenly spaced projections over 360°, we use linear interpolation to estimate the intensity values of undersampled rays near the edges. After reconstruction, OD

images are converted to dose by normalizing to the true dose at a known point (D_{max})[13, 17]. This allows comparison of measured and true dose along the diameter of the dosimeter, as show in Figure (8).

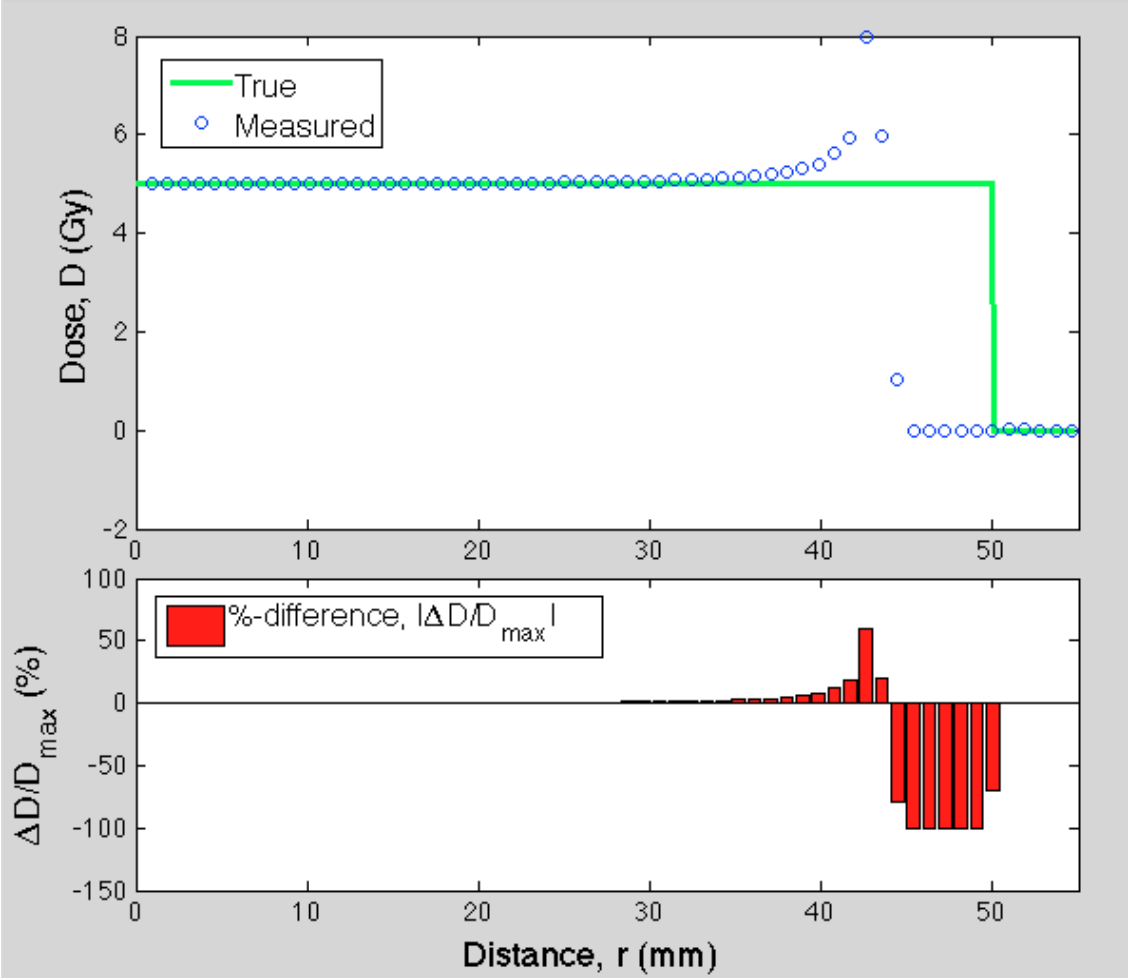

Figure 8: Methodology for determining the usable radius. This is an expansion of the dose comparison panel from Figure 5, showing the true and measured dose Gy and the percent difference normalized to reference dose Dmax. To measure the usable radius, the lower panel is expanded and the cursor tool used to locate the furthest distance in mm where the percent difference is less than ±2%.

2.1.3 Extension of Previous Work for this Thesis

For this thesis, ScanSim's capabilities were expanded to accommodate the geometry and physics of dry scanning. Parameters for the solid-tank well size and refractive index were added to the GUI, and an extra media interface representing the solid-tank-fluid boundary added to the supporting functions for ray tracing.

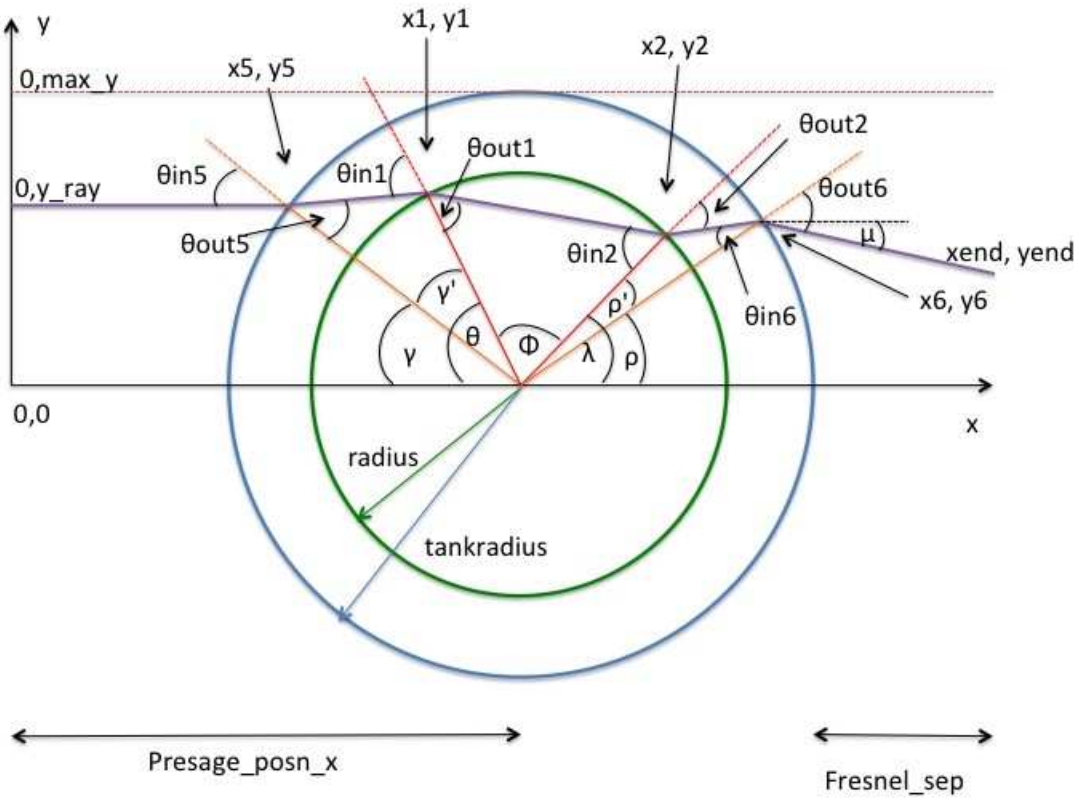

Figure 9: Solid-tank geometry used to determine independent ray paths. ScanSim uses Snell's Law and basic geometry to calculate each angle and the x,y coordinates of media boundary points. Lines are drawn between known points to form the ray tracing. Information about the ray intensity, transmission coefficients, and attenuation is updated at each media boundary.

Because total internal reflection is a larger concern with the extra media interface

and greater range of refractive indices allowed, this effect was accommodated for all media interfaces. Total internal reflection occurs when the angle of incidence on a media interface is greater than the critical angle dictated by the refractive index of the two media:

$$\theta_c = \arcsin(\frac{n_2}{n_1}) \tag{6}$$

At each media interface, the angle of incidence is compared to the critical angle for the boundary. If the incident angle exceeds the critical angle, that ray was declared scattered and non-recoverable, and the ray truncated at the point of incidence. The prior version of ScanSim (used to simulate the ideal system type) did not account for scatter rejection by the telecentric collimators and lenses used with this system, and all rays were declared detectable regardless of their angle of incidence on the detector or magnitude of intensity loss. In the updated telecentric version (used to simulate the telecentric system type), rays are only declared detectable if their angle of incidence on the detector is less than or equal to the telecentric lens tolerance. Any rays not meeting this criterion are considered rejected, and their final intensity values set to zero. Rejected rays are visualized on the ray tracing output diagram with dotted lines for scattered events and "X" marks for total internal reflection.

2.2 Scanning and Simulation Parameters

The controlled variables of the simulations were the system type (telecentric or

ideal), refractive indices of the dosimeter (1.5-1.47) and surrounding fluid (1.55-1.0), the gap size between the dosimeter and the solid-tank well (1.0-5.0mm), and the telecentric lens tolerance (0.5-5.0°). Gap size refers to the difference between the solid-tank well radius, r_t, and the dosimeter radius, r_0, and is a measure of how tightly the dosimeter fits into the solid-tank well. System types are further explained in Section 2.2.1.

A total of five scanning configurations were investigated to evaluate the effects of these parameters on the accuracy of the system. These configurations are summarized in Section 2.3.

All scanning configurations were simulated with 0.2mm ray spacing and a uniform dose distribution of 5Gy to the total dosimeter volume. The ray spacing value was chosen to provide good sampling of the dose distribution without requiring lengthy calculation times—since each ray path is calculated independently, calculation times are very dependent on the number of rays, which is determined by the ray spacing. A uniform dose distribution was chosen to make measurement of the usable radius more straightforward. Reconstruction was relative to match actual scanning procedures, and by filtered backprojection. While ScanSim is capable of algebraic reconstruction techniques, this method is slow and computationally intensive, making it inefficient considering the number of simulations required for this work.

2.2.1 System Types

Two types of system were investigated in this thesis. An ideal system is one in

which all rays are declared detectable, regardless of refracted angle or intensity loss. This means that, because intensity information, transmission factors, and attenuation are stored for each stage of a ray's journey through the media, any information gathered along the ray path can be used in reconstruction, regardless of the outcome of the ray path. This system type is used as a method of comparison for a telecentric system. An ideal system is not unfeasible in reality if the dosimeter dimensions are known and the trajectory of the rays can be calculated a-priori—both of which are feasible for cylindrical dosimeters[13]. In a telecentric system, any ray that could not feasibly be detected in a telecentric setup is not used in reconstruction. This includes any ray which experiences total internal reflection, or whose angle of incidence on the detector exceeds the telecentric lens tolerance. In the telecentric system type, this is achieved by setting the stored intensity values of these rejected rays to zero.

2.2.2 Solid-tank and Dosimeter Properties

The simulated dosimeter parameters are common to PRESAGE® radiochromic dosimeters used in RPC head phantoms in order to maintain relevancy. The fixed dosimeter properties[17] were radius, r_0 = 50mm, OD sensitivity = 0.023cm^-1 Gy^-1, and unirradiated background OD = 0.003cm^-1. The refractive indices (ranging from 1.47-1.5) and other simulated dosimeter properties were chosen based on the measured properties of a sample of PRESAGE® dosimeter formulations[10].

The simulated solid-tank parameters were chosen based on the physical solid-

tank system DFOS. The simulation does not currently include the media boundary between the air and the edges of the solid-tank; because the rays are parallel collimated, there would be minimal refraction or reflection at this interface. It also does not include parameters for the amount of solid-tank the ray must travel through before reaching the fluid gap boundary. The refractive index was fixed for all simulations at $RI_t = 1.5$.

2.3 Scanning Configurations

Five scanning configurations were simulated—two configurations for an ideal system and three configurations for a telecentric system. Fixed and controlled variables for each configuration are summarized in Table (1) below. Scanning configurations fall into three categories:

Optimal media matching: these simulations attempt to determine the appropriate choice of RI-matched fluid based on the dosimeter and solid-tank RI. For each chosen dosimeter-tank RI pair, the fluid RI value was varied.

Effect of gap size: these simulations evaluate the effect of scanner geometry on our chosen metric. We attempt to determine an optimal fluid RI choice based on the dosimeter and solid-tank RI, and the "fit" of the dosimeter in the solid-tank well by changing the gap size parameter. For each dosimeter-tank pair, a gap size was chosen and the fluid RI varied. These simulations were repeated for each gap size in the specified range.

Telecentric lens tolerance: these simulations evaluate the effect of increasing or

decreasing the telecentric lens tolerance on our metric. For each dosimeter-tank pair, a telecentric lens tolerance was chosen and the fluid RI varied. These simulations were repeated for each telecentric lens tolerance in the specified range.

Table 1: Scanning Configuration Summary. Each scanning configuration fits into one of three categories: optimal media matching, effect of gap size, or telecentric lens tolerance. Two configurations were evaluated for the ideal system type, and three configurations evaluated for the telecentric system type.

System Type	Category	Fixed Variables	Controlled Variables
Ideal System	Optimal Media Matching	Solid-tank RI = 1.5 Gap Size = 1.0mm	Dosimeter RI (1.5-1.47) Fluid RI (1.55-1.0)
	Effect of Gap Size	Solid-tank RI = 1.5 Fluid RI = 1.5	Dosimeter RI (1.5-1.47) Gap Size (1.0-5.0mm)
Telecentric System	Optimal Media Matching	Solid-tank RI = 1.5 Gap Size = 1.0mm Lens Tolerance = 1.0°	Dosimeter RI (1.5-1.48) Fluid RI (1.55-1.33)
	Effect of Gap Size	Solid-tank RI = 1.5 Lens Tolerance = 1.0°	Dosimeter RI (1.5-1.48) Fluid RI (1.51-1.45) Gap Size (1.0-5.0mm)
	Telecentric Lens Tolerance	Solid-tank RI = 1.5 Gap Size = 1.0mm	Dosimeter RI (1.5-1.48) Fluid RI (1.51-1.33) Lens Tolerance (0.5-5.0°)

2.4 Metrics for Evaluation

The primary metric used to evaluate the accuracy of the system is the *usable radius*, r_u. The usable radius is the distance in millimeters from the center of the

dosimeter at which the measured and true dose differ by less than 2%. The reference dose for percentage difference is $D_{\max}$. Because all scanning configurations were evaluated with a simulated uniform dose distribution of 5Gy to the total dosimeter volume, $D_{\max}$ = 5Gy. In this thesis, this value is expressed as the percentage ratio of the usable radius to the dosimeter radius $\left(\frac{r_u}{r_0} * 100\right)$ for dimensionless comparison.

2.4.1 Other Terms

Optimal Fluid RI: the fluid refractive index required to achieve the maximum usable radius for a given dosimeter-tank pair with the current scanning configuration.

Maximum Usable Radius: the usable radius achieved with optimal media matching for the given scanning configuration.

Recoverable Scatter: when rays scattered at an initial media interface are refracted back into telecentric alignment before reaching the detector.

3. Results and Discussion

Results in this chapter are presented for the effect on the usable radius for the five scanning configurations summarized in Section 2.3. Section 3.1 includes results for the ideal system type, while Section 3.2 includes results for the telecentric system type. Results are further broken down by configuration category (optimal media matching, effect of gap size, and telecentric lens tolerance) within each system type. Usable radius measurements were made using the technique described in Section 2.4. Unique ring artifacts appeared in the reconstructed images at certain media combinations, and are discussed in Section 3.3. Finally, comparison between an ideal system and a telecentric system of the maximum achievable usable radius for a variety of dosimeter refractive indices is presented in Section 3.4.

3.1 Ideal System

3.1.1 Optimal Media Matching

The usable radius for a variety of dosimeter RIs in an ideal system is presented graphically in Figure (10), and the maximum usable radius for each dosimeter is shown in Table (2).

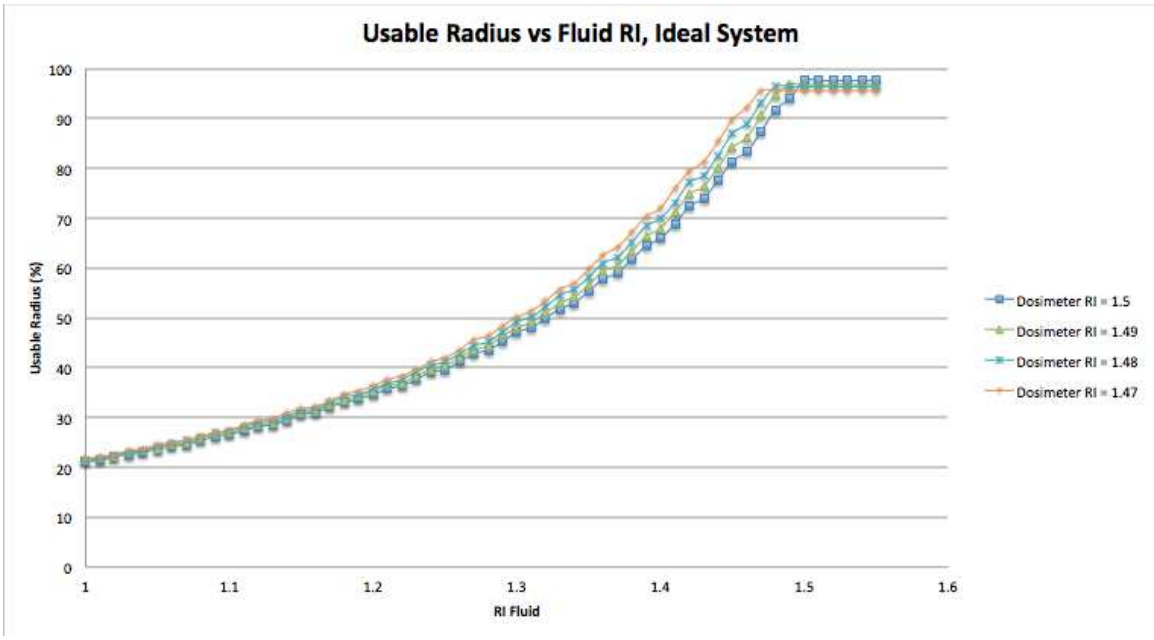

Figure 10: The effect of media mismatches on the usable radius for an ideal system. Gap size = 1mm, Solid-tank RI = 1.5.

For each dosimeter, the maximum usable radius is achievable with any fluid RI choice with a refractive index greater than or equal to the dosimeter. When the fluid RI is greater than or equal to the dosimeter is it unlikely or impossible for a ray to experience total internal reflection until it has passed through the dosimeter volume. With the ideal system, this means that the ray would still contain enough intensity information to successfully reconstruct the dosimeter volume. Once the fluid RI drops below the RI of the dosimeter, the usable radius decreases non-linearly. Perfect media matching results in the highest maximum usable radius of 97.6%, with a linear decrease as the dosimeter RI decreases. Over the range of dosimeter RIs examined, the maximum usable radius decreased from 97.6% to 95.6%.

Table 2: Maximum Usable Radius by Dosimeter RI, Ideal System

Dosimeter RI	Max. Usable Radius
1.5	97.6%
1.49	96.8%
1.48	96.4%
1.475	96.0%
1.47	95.6%

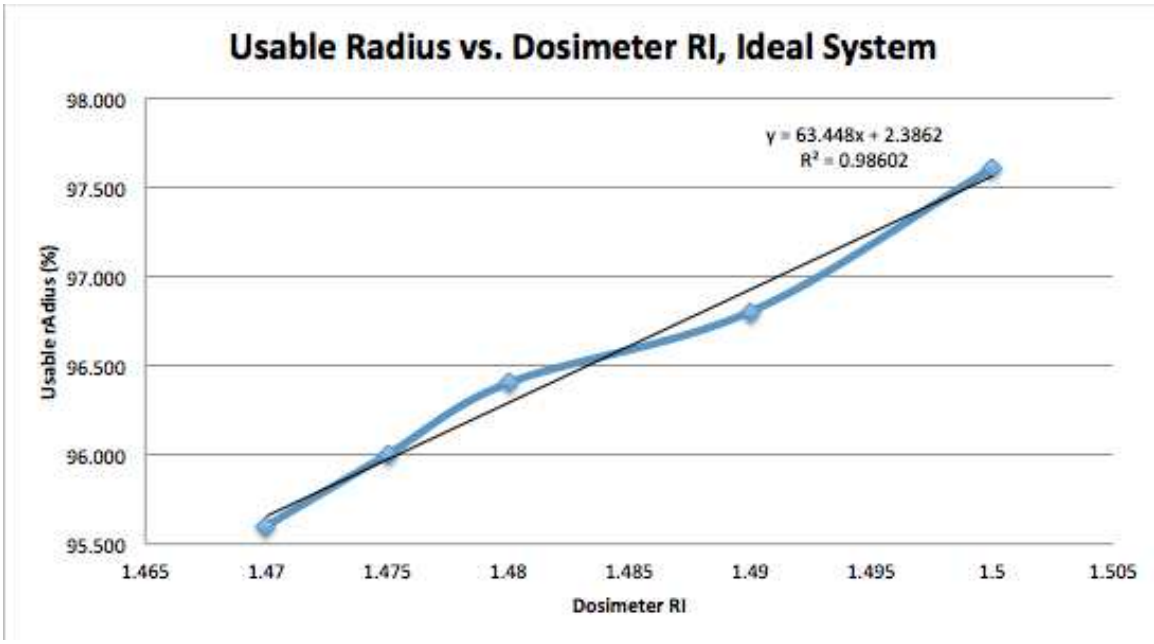

Figure 11: Linear relationship between maximum usable radius and dosimeter RI for an ideal system. Solid-tank RI = 1.5, Fluid RI = optimal fluid RI

For an ideal system where scattered light is collected and used in reconstruction, most of the dosimeter produces accurate dose measurements, even when the dosimeter and solid-tank are mismatched. As the fluid RI decreases, transmission losses and total internal reflection decrease the usable portion of the dosimeter. These results suggest that dry scanning with ideal detectors could eliminate the need for fluid matching

altogether by simply using a fluid with a higher refractive index than the dosimeter.

3.1.2 The Effect of Gap Size

The results of simulations investigating the effect of gap size on the usable radius are shown in Figure (12). The maximum usable radius exhibits a strong linear relationship with gap size for all dosimeter refractive indices. As the gap size increases, the ray path length through the fluid increases, amplifying any refraction effects and increasing transmission losses at boundaries. However, for perfect media matching we would not expect a decrease in the usable radius—this is an artifact of the simulation, where due to the increased gap size, fewer rays are passing through the dosimeter. See Appendix B, Figure (28) for a ray-tracing illustration of this effect.

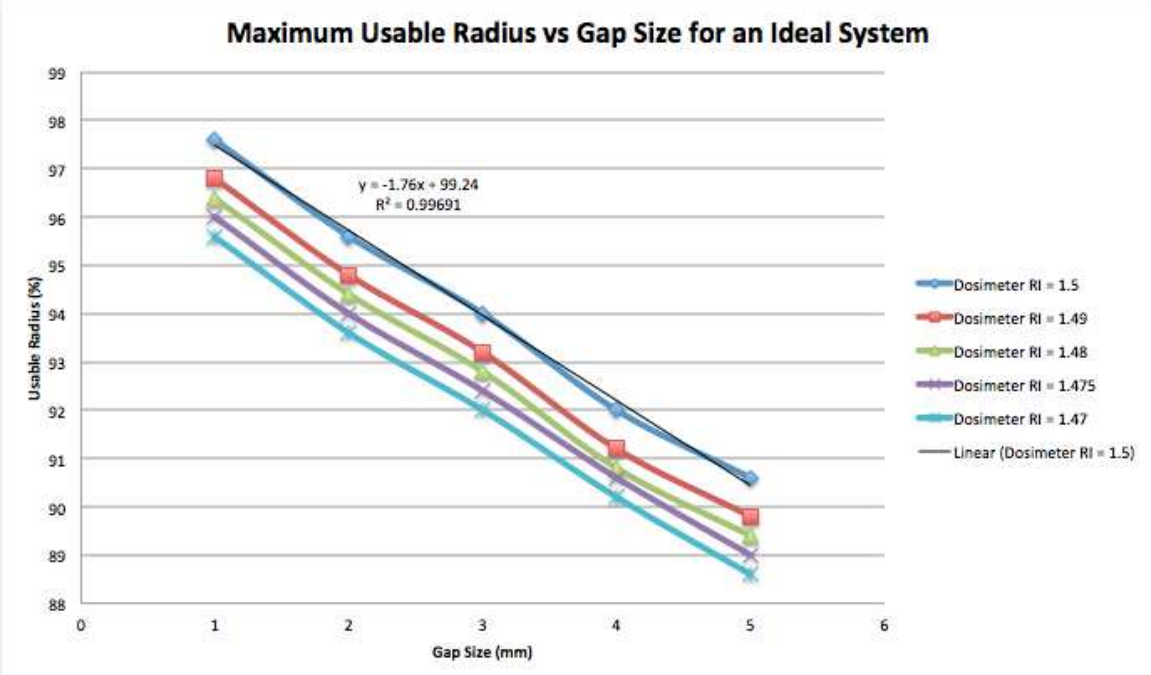

Figure 12: The effect of changing gap size on the usable radius for ideal

systems. Solid-tank RI = 1.5, gap size = 1mm, fluid RI = 1.5

3.2 Telecentric System

3.2.1 Optimal Media Matching

Results showing the usable radius for a range of fluid RI choices and dosimeters are displayed in Figure (13). Again, a scanning scenario with perfectly matched dosimeter and solid-tank produces the highest maximum usable radius, with a linear decrease in maximum usable radius as the dosimeter RI decreases.

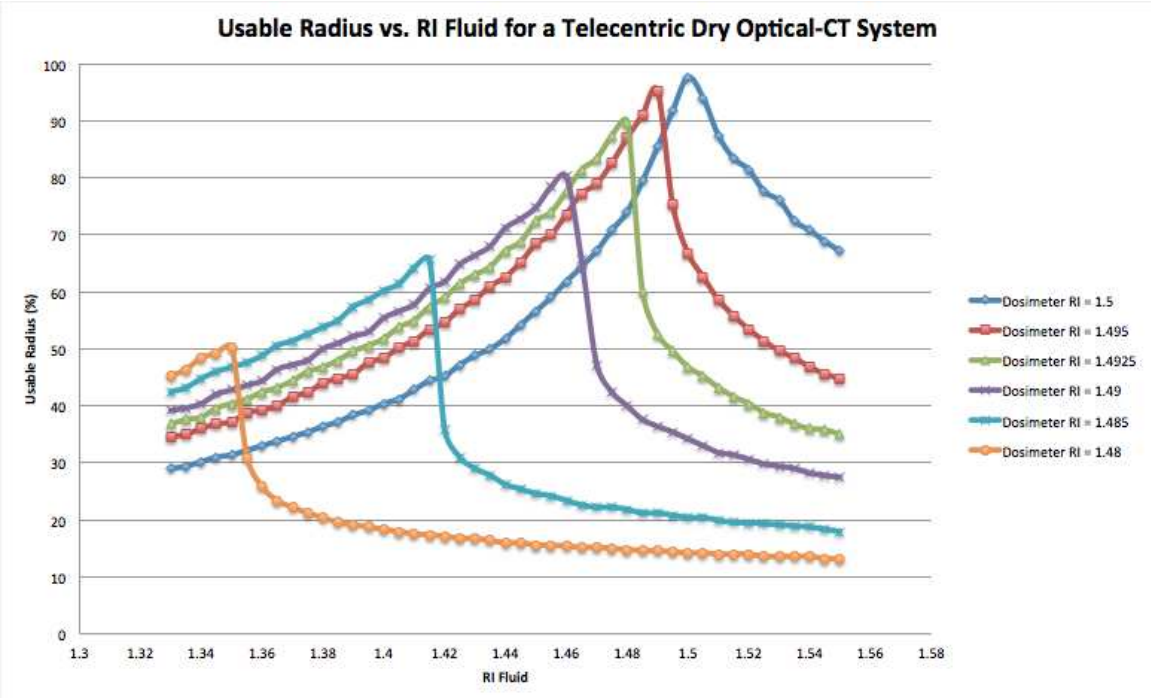

Figure 13: Media matching in a telecentric system. Gap size = 1mm, Solid-tank RI = 1.5, Lens Tolerance = 1.0°.

Unlike an ideal system, when the fluid refractive index is greater than the

dosimeter, there is a sharp falloff in the usable radius for a telecentric system caused by unrecoverable scatter on the edges of the dosimeter. As rays exit the dosimeter into a fluid with a higher refractive index, they are bent towards the normal in accordance with Snell's Law (Eq. 1). Near the edges of the dosimeter, the angle of the normal line is such that these rays are bent even further out of alignment with the telecentric tolerance. This effect occurs in reverse as the fluid refractive index matches the dosimeter and continues to decrease, and eventually those refracted rays are bent away from the normal enough to come into telecentric alignment, causing a sharp peak in the usable radius. The rays near the center of the dosimeter are not deflected as much by media mismatches because their incident angles are much smaller, so they generally remain detectable for all scenarios. Because of this recoverable scatter effect, the optimal fluid RI is not a match with either the dosimeter or the solid-tank, but occurs at a lower refractive index than either, as shown in Figure (14).

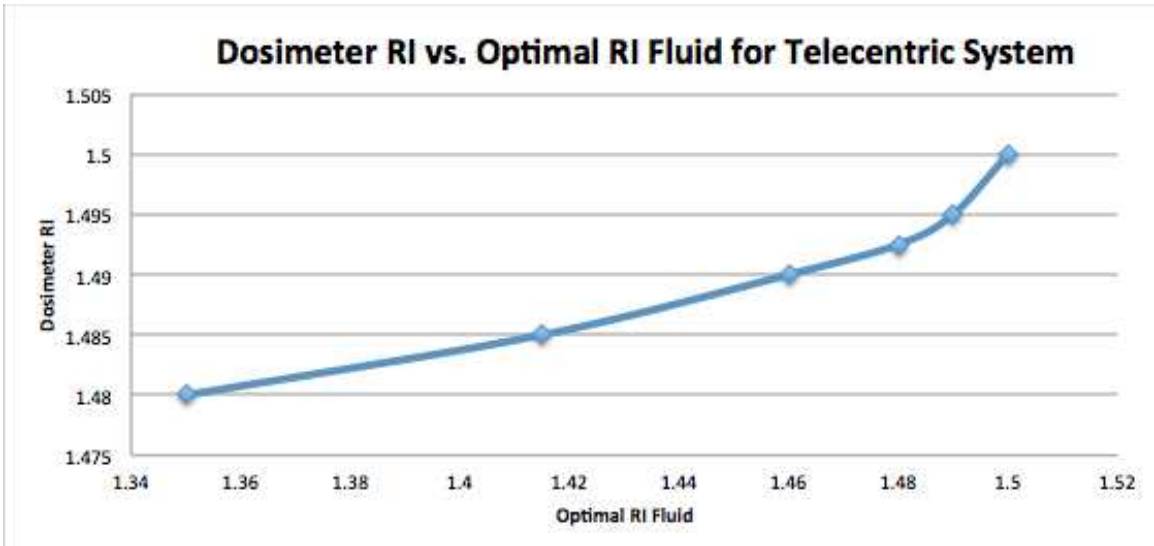

Figure 14: Optimal fluid RI for Telecentric System. Solid-tank RI = 1.5, Gap Size = 1.0mm, Lens Tolerance = 1.0°.

Once the fluid RI continues to decrease past the optimal value, rays continue to be refracted towards telecentric alignment, creating the milder decrease in usable radius shown in Figure (13).

The maximum usable radius decreases from 97.6% to 50.2% over a change of 0.02 in dosimeter refractive index, indicating that telecentric dry scanning is extremely sensitive to media mismatches between the dosimeter and solid-tank. Figure (15) displays the relationship between the maximum usable radius and the RI of the dosimeter. Mismatches between the tank and dosimeter cause more scatter, which decreases the number of rays detected by the telecentric lens.

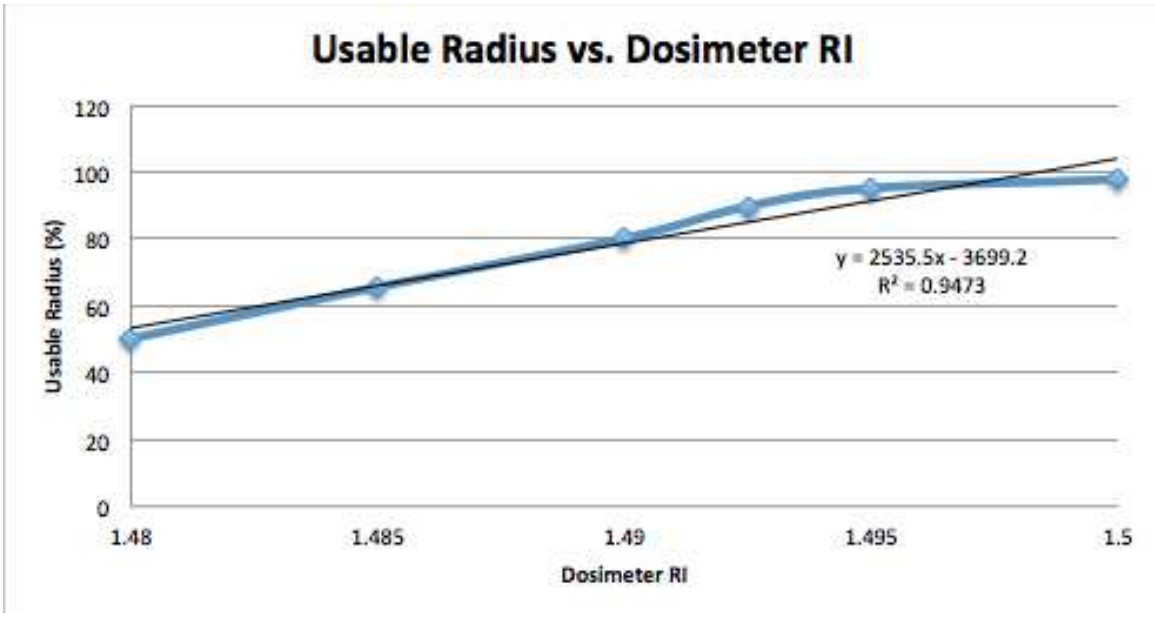

Figure 15: Maximum usable radius for various dosimeter RIs in a telecentric system. Solid-tank RI =1.5, Gap Size = 1.0mm, Lens Tolerance = 1.0°, Fluid RI = optimal value.

Ray tracings demonstrating standard results for various media combinations in a telecentric system are provided in Appendix B, Figures (29)-(31).

3.2.2 The Effect of Gap Size

Figures (16)-(18) show the effect of changing gap size on the usable radius for select dosimeter RIs in a telecentric system. For a given dosimeter RI, the gap size has drastic effects on the usable radius with no apparently quantifiable relationship.

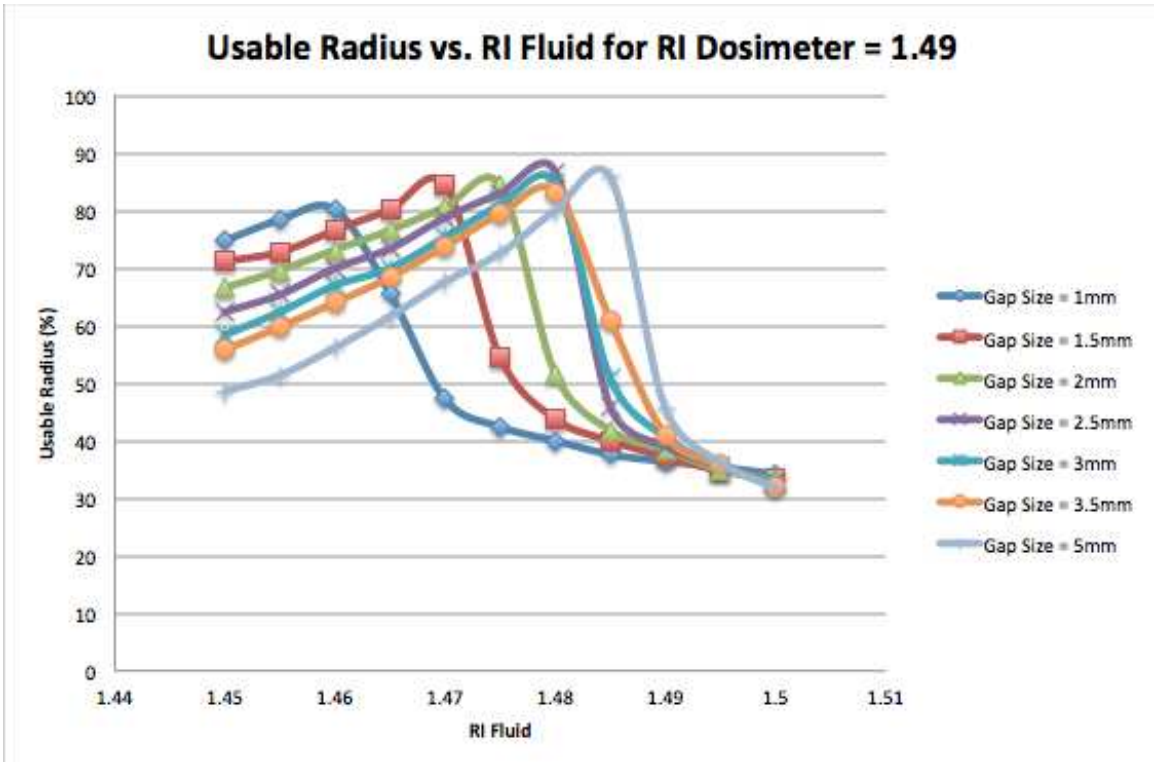

Figure 16: The effects of gap size on the usable radius for a telecentric system with dosimeter RI =1.49, and solid-tank RI = 1.5. Lens tolerance = 1.0°.

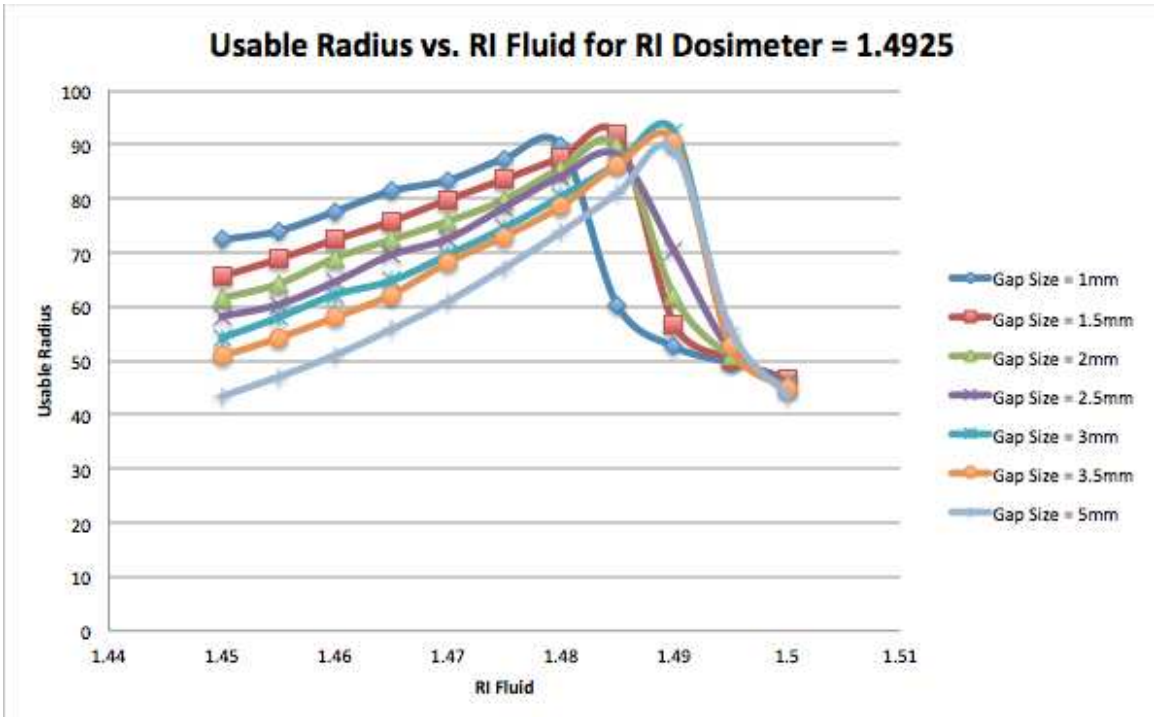

Figure 17: The effects of gap size on the usable radius for a telecentric system with dosimeter RI = 1.4925 and solid-tank RI = 1.5. Lens tolerance = 1.0°.

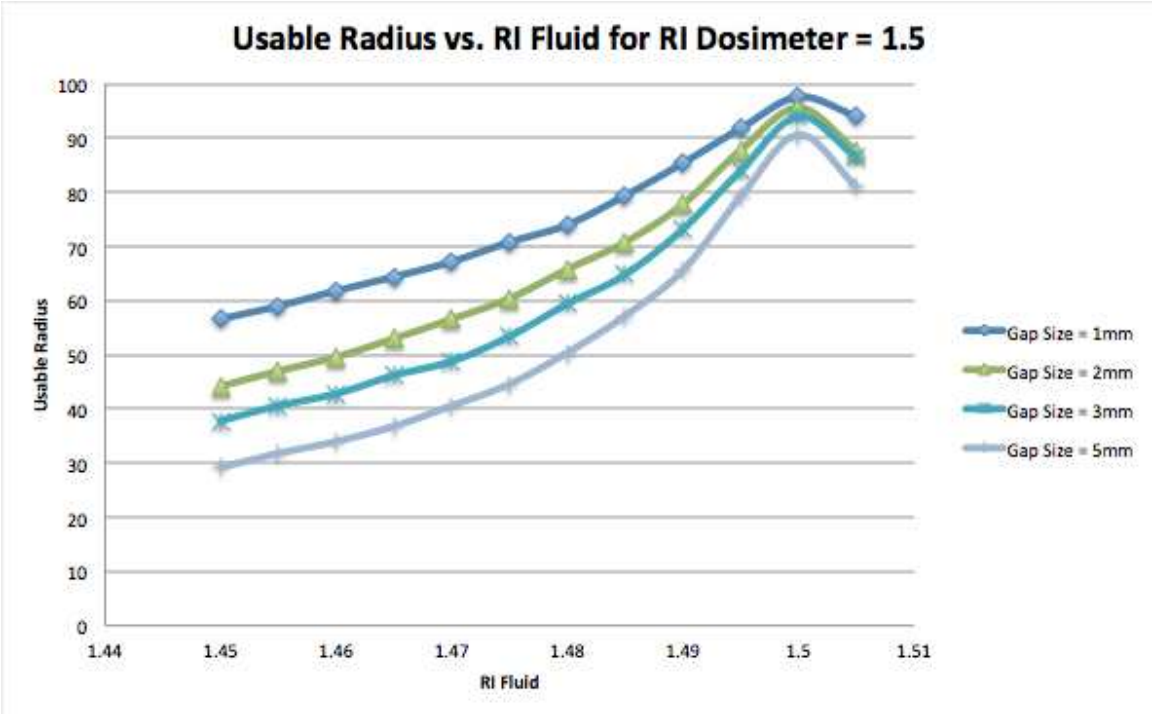

Figure 18: The effects of gap size on the usable radius for a telecentric system for perfectly matched dosimeter and solid-tank at RI = 1.5. Lens tolerance = 1.0°.

Generally, the optimal fluid RI increases as the gap size increases, becoming more closely matched to the dosimeter at large (>3mm) gap sizes. The results suggest that the maximum usable radius depends on gap size in addition to dosimeter-tank mismatch. At larger gap sizes, refraction effects (including recoverable scatter) are amplified by in the increased amount of fluid traveled by a light ray. As a result, changing the gap size by a small amount can cause significant increases in the usable radius. For example, in Figure (16) above, the usable radius increases from 47.2% with a gap size of 1mm to 84.4% with a gap size of 1.5mm for the exact same RI combination of $RI_t = 1.5$, $RI_{dosimeter} = 1.49$, and $RI_{fluid} = 1.47$.

Figure (19) shows how the optimal fluid RI relates to gap size for mismatched dosimeter-tank RIs. Consistent with earlier results, as the gap size increases, the optimal fluid RI becomes more closely matched to the dosimeter. At small gap sizes, the optimal fluid RI is much lower than the dosimeter RI.

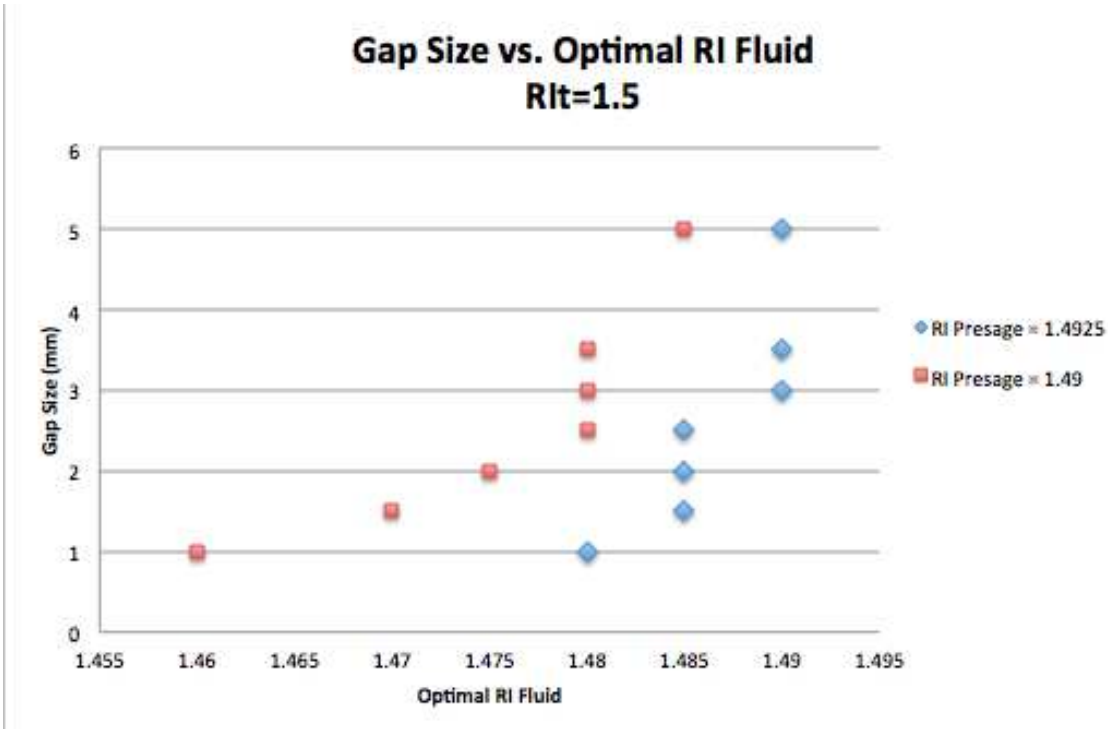

Figure 19: Optimal fluid RI choice based on gap size for mismatched dosimeter and solid-tank. Solid-tank RI = 1.5, Lens tolerance = 1.0°.

Figures (25)-(27) in Appendix A show an alternate arrangement of the data for these dosimeters examining the relationship between usable radius and gap size for various fluid RIs. Ray tracings demonstrating some of these results are provided in Appendix B, Figures (32) and (33).

3.2.3 Telecentric Lens Tolerance

The usable radius for various refractive media combinations at different telecentric lens tolerances is shown in Figure (20). At higher tolerance (>5°), a telecentric system behaves similarly to an ideal system because it is accepting much more scattered light that would be rejected at a lower tolerance.

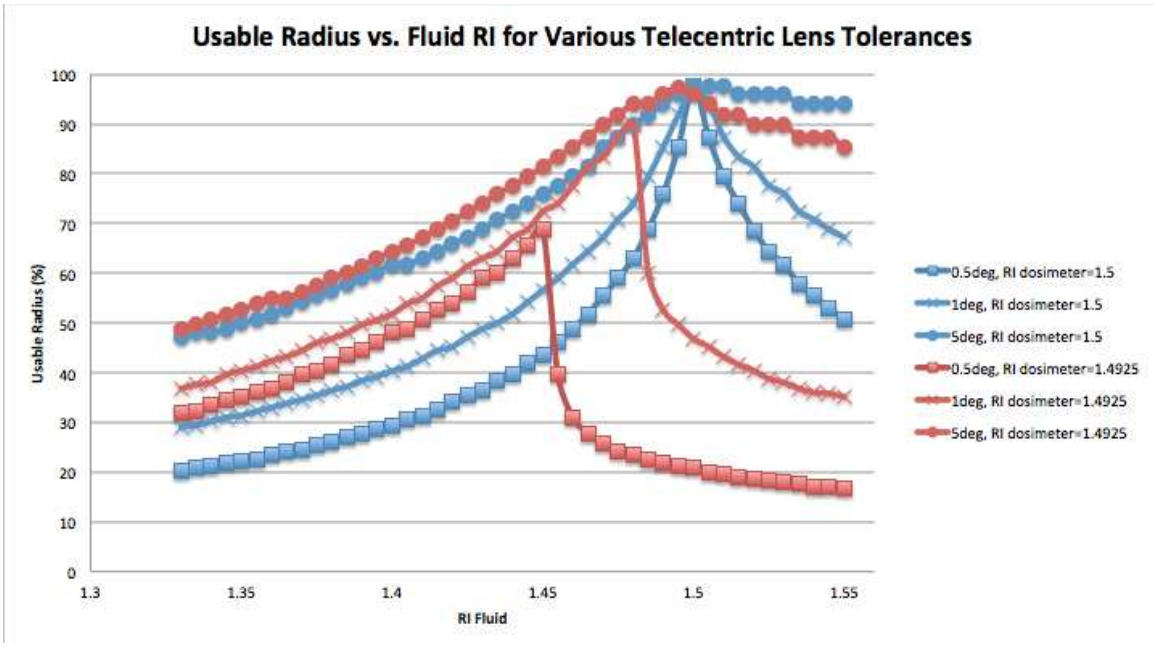

Figure 20: Effect of changing telecentric lens tolerance on usable radius. Gap size = 1mm, Solid-tank RI = 1.5.

Figure (21) compares the maximum usable radius for matched and mismatched dosimeters at different telecentric lens tolerances. For perfectly matched media, the usable radius remains at 97.6% for all telecentric lens tolerances. For mismatched dosimeter-tank RI and high telecentricity (low tolerance), the maximum usable radius increases rapidly from 68.8% at 0.5° to 89.8% at 1.0°. The maximum usable for mismatched media approaches that of perfectly matched media at large telecentric lens

tolerances (>2.0°), indicating that slight spoiling of the telecentric beam (increasing the lens tolerance) can recover the usable radius in situations where the solid-tank and dosimeter are slightly mismatched.

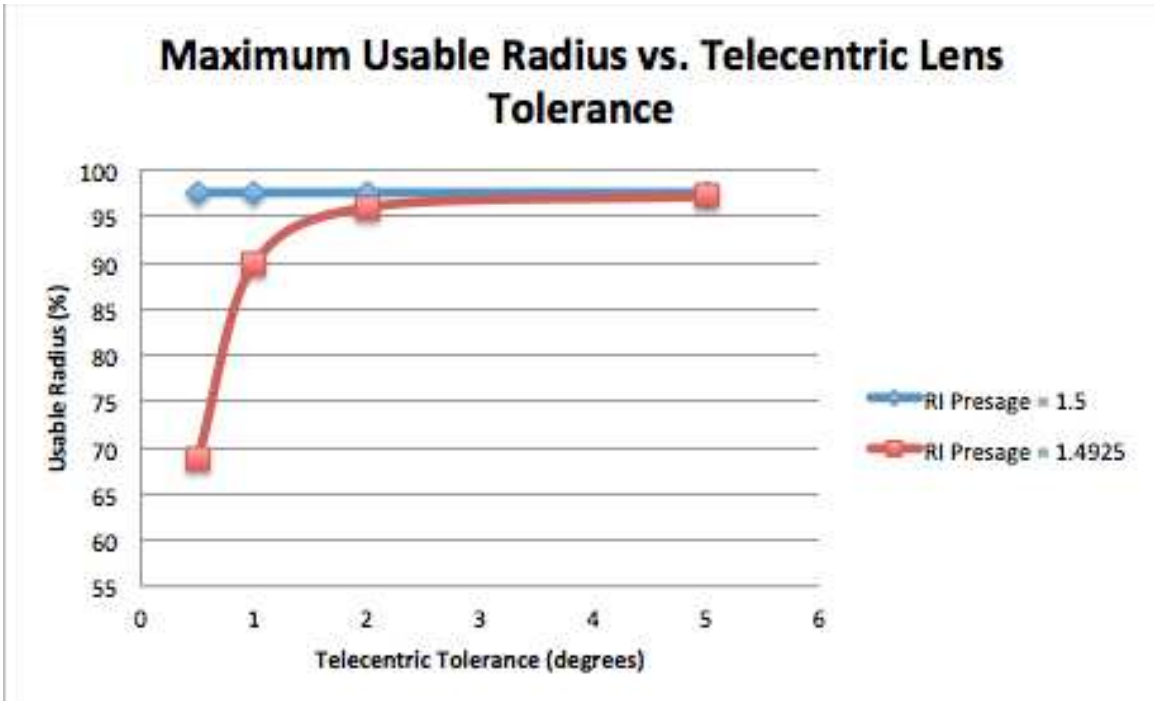

Figure 21: Usable radius for perfectly matched and mismatched media at different telecentric lens tolerances

3.3 Unique Artifacts

At certain refractive media combinations, a unique ring artifact appears in the reconstructed image, as shown in Figure (22).

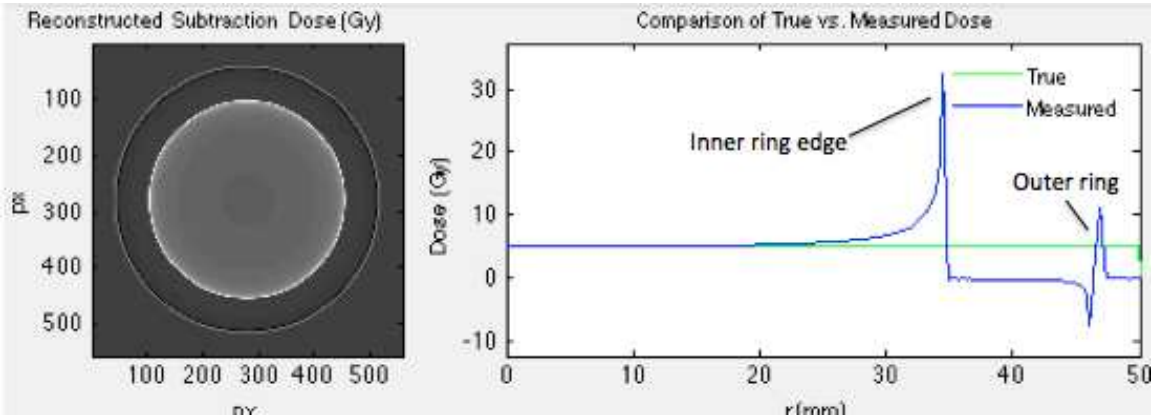

Figure 22: Ring artifacts in reconstructed image of the ray tracing in Figure (23). The outer ring is caused by recoverable scatter near the edges. Dosimeter RI = 1.48, Fluid RI = 1.45, Solid-tank RI = 1.5. Gap size = 1mm, Telecentric Tolerance = 1.0°

This outer ring in the Figure above corresponds to rays near the edge of the dosimeter being detected while those on either side do not due to the geometry and media RI combinations. The inner ring represents the central core of rays that experience little deflection and are generally detectable at all media combinations. The ray-tracing diagram that produced the reconstructed image in Figure (22) is shown in Figure (23). The ring disappears when the fluid RI decreases to the optimal value, making it a potentially useful landmark for trial-and-error fluid matching.

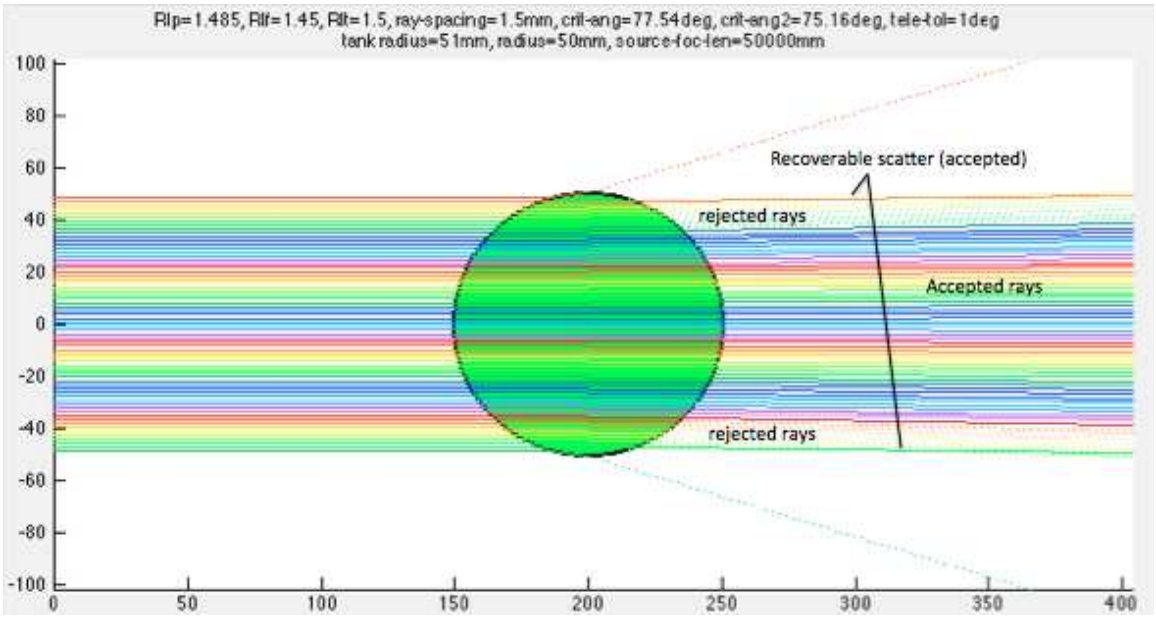

Figure 23: Ring artifacts caused by recoverable scatter at the edges of the dosimeter. Solid lines are rays accepted by the telecentric lens, and dotted lines are rejected. The gap size is 1mm, so it is not visible in this image.

3.4 Comparison between Telecentric and Ideal Optical-CT Systems for Dry Scanning

The result of a comparison of the maximum usable radius for an ideal and a telecentric system is shown in Figure (24) and Table (3). For matched media, the telecentric system and ideal system perform identically with 97.6% of the dosimeter radius measured accurately.

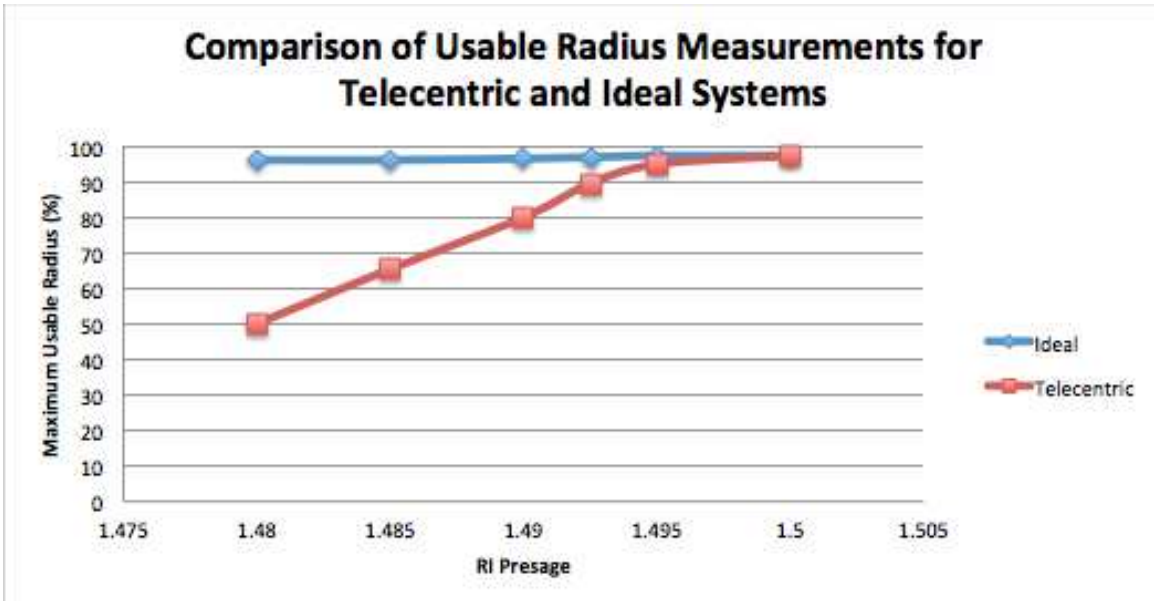

Figure 24: Maximum usable radius comparison between telecentric and ideal system

For mismatched media, the increased amount of rejected scatter in a telecentric system causes a significant drop in the maximum usable radius compared to the ideal system from 2.5% difference at 0.005 difference in refractive index to 63.0% difference at 0.02 difference in refractive media.

Table 3: Media mismatching and effects on the maximum usable radius: a comparison of ideal and telecentric systems

	Ideal System	Telecentric System	
Magnitude of Mismatch	Maximum Usable Radius (%)		Percentage Difference
0.0	97.6	97.6	0.00
-0.005	95.2	97.6	2.49
-0.01	80.2	96.8	18.76
-0.015	65.6	96.4	38.02
-0.02	50.2	96.4	63.03

4. Conclusions

The aims of this thesis were to investigate the feasibility of dry telecentric optical-CT imaging and determine optimal design and scanning parameters for such a system by simulating common scanning configurations. Initial results show that dry optical-CT imaging is feasible in situations when the dosimeter and solid-tank have closely matched refractive indices or if data is not required in the periphery of the dosimeter. If the absolute magnitude of dosimeter-tank RI mismatch is less than -0.01 , a dry telecentric scanning system will produce dose measurements within ±2% of the true dose across over 80% of the dosimeter radius. To produce accurate dose measurements across 95% of the dosimeter radius with a dry telecentric system, the absolute dosimeter-tank mismatch must be less than -0.005. In situations with dosimeter-tank RI mismatches greater than -0.01, dose measurements in the periphery will be inaccurate. However, increasing the telecentric lens tolerance to 1.0° or higher by spoiling the beam with a diffuser or increasing the aperture stops in the lens could help recover the usable radius when the absolute dosimeter-tank RI mismatch is greater than -0.01, further improving the feasibility of this technique.

The simulation tool ScanSim proved to be very useful in estimating the optimal choice of RI of the small amount of fluid still required for dry scanning. As demonstrated in the results, the optimal fluid RI choice is not immediately obvious in situations when the dosimeter and tank are not refractively matched, as it is a function

both of the dosimeter-tank RI mismatch and the gap size. Generally, if the gap size is large (>5mm), the optimal fluid RI choice will be slightly lower than but closely matched to the dosimeter RI. At small gap sizes (1-3mm), the optimal fluid RI choice is considerably lower than the dosimeter RI. For all gap sizes, greater mismatches between the dosimeter and solid-tank RIs result lower optimal fluid RI choices. A quantitative function describing the relationship between dosimeter-tank RI mismatch and gap size could be very beneficial both for increasing the capabilities of the ScanSim tool and for eliminating the need for any trial-and-error fluid matching for this system. Until then, fluid-matching efforts could take advantage of the unique ring artifacts that appear at certain media combinations to confirm an optimal fluid RI choice based on these simulations.

There are several future directions that could be explored to further the results of this work. One of benefits of the solid-tank is the removal of imperfections in the tank from the final image by subtracting the pre-scan flood image. However, using this technique for dry scanning is problematic because good quality flood images require fluid refractively matched to the solid-tank, while good quality scans require a fluid whose RI is based on the refractive mismatch between the dosimeter and tank. The use of two different fluids in the flood scan and imaging scans causes reconstruction corrections to be inaccurate. Additional simulations could be done to determine an optimal average fluid RI that could be used in both flood and imaging scans to produce

accurate reconstruction corrections without sacrificing image quality in the form of decreased usable radius. Alternatively, investigation into a reconstruction algorithm that does not make use of flood images at all could potentially eliminate this concern. Also of high priority is an investigation of the effects of changing the solid-tank refractive index, which was held fixed at 1.5 for these simulations to match the physical system. Usable radius measurements are not dependent on the relative difference between the refractive indices of the solid-tank and dosimeter. If the dosimeter has a higher refractive index than the solid-tank, the effect on the usable radius and optimal fluid RI choice for that configuration are currently unknown.

Appendix A

The following figures display data from Section 3.2.2 in an alternate manner to more closely examine optimal fluid RI choices based on gap size for a telecentric system. Figure (27) shows that when all media are perfectly matched, the telecentric system behaves identically to the ideal system. When the dosimeter and solid-tank are refractively matched, there is a linear relationship between gap size and usable radius for any fluid RI choice. When the dosimeter and tank are mismatched, there appears to be no quantifiable relationship between usable radius, gap size, and fluid RI choice.

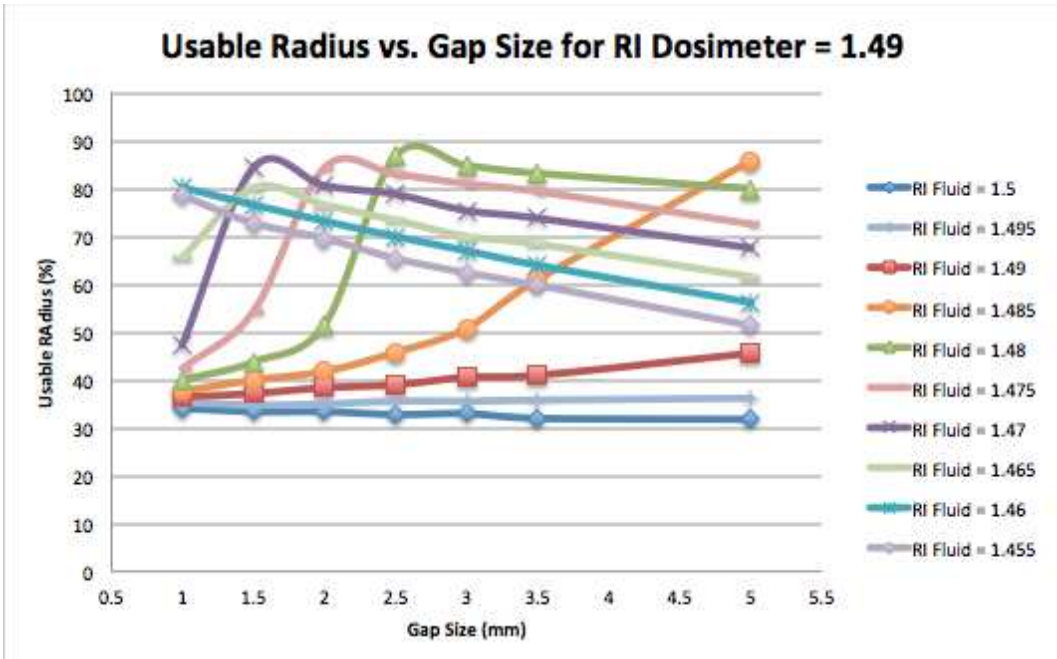

Figure 25: Relationship between usable radius and gap size for various fluid RI choices in a telecentric system. Dosimeter RI = 1.49, solid-tank RI = 1.5

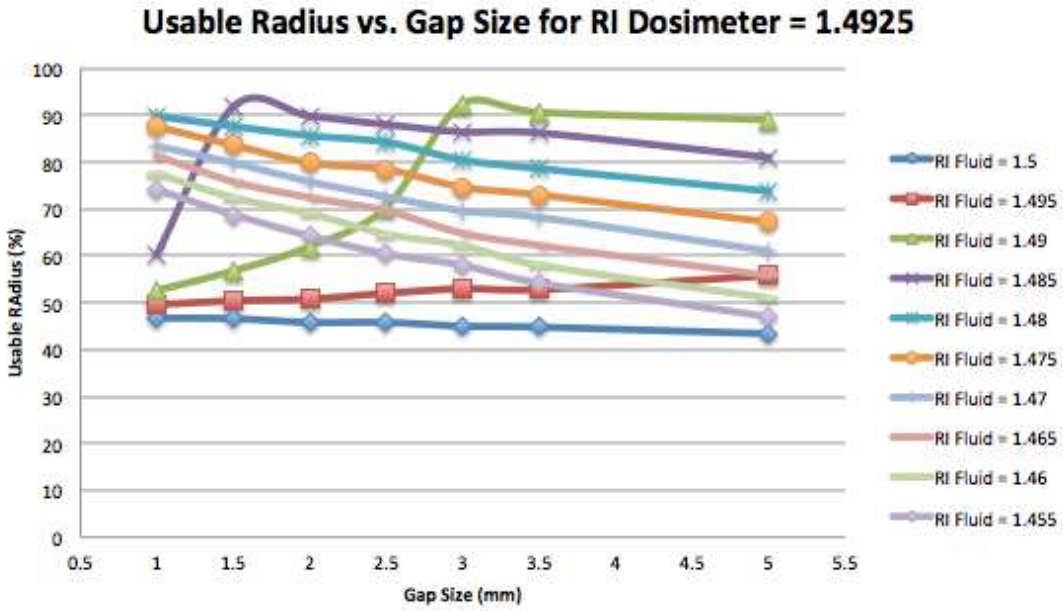

Figure 26: Relationship between usable radius and gap size for various fluid RI choices in a telecentric system. Dosimeter RI = 1.4925, solid-tank RI = 1.5

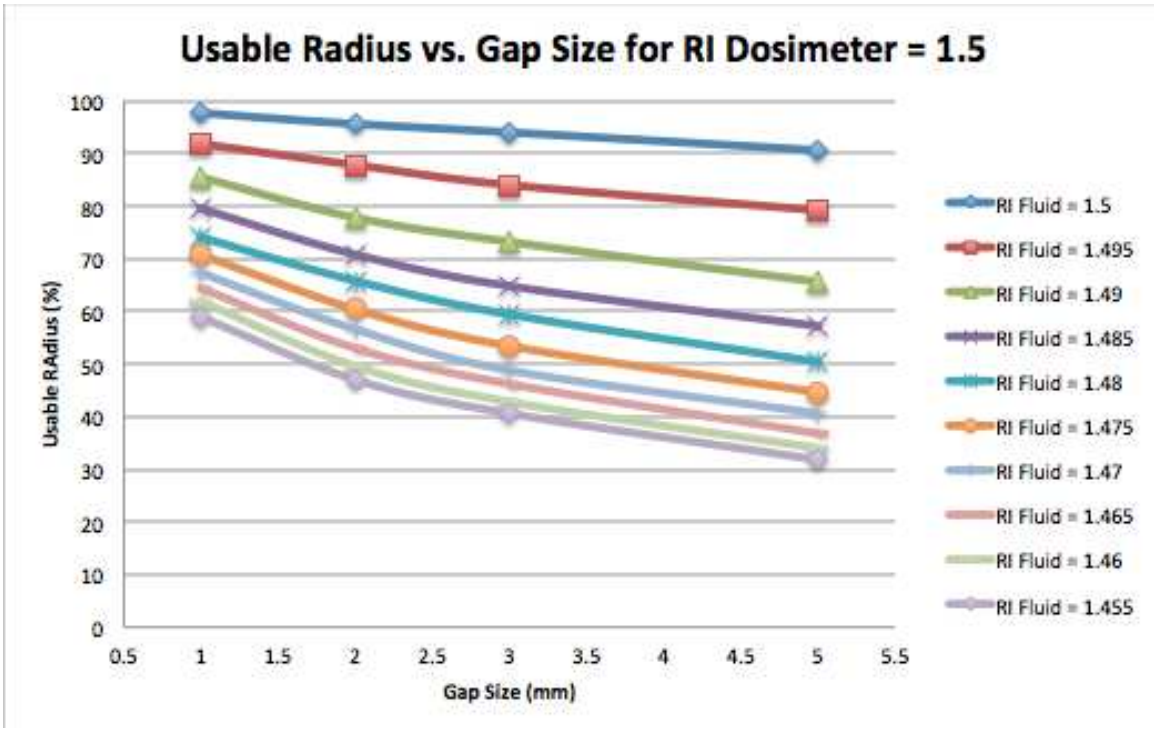

Figure 27: Relationship between usable radius and gap size for various RI fluid choices in a telecentric system. Perfect media matching between dosimeter and tank at RI = 1.5

Appendix B

This section contains additional figures illustrating ray tracings for standard results and special effects discussed in Chapter 3.

Figure (28) demonstrates the gap size effects discussed in Section 3.1.2. As the gap size increases, the number of rays passing through the dosimeter decreases, causing a decrease in the usable radius even with perfectly matched media. This is easiest to visualize in the transmission coefficients plot to the left of the ray tracing.

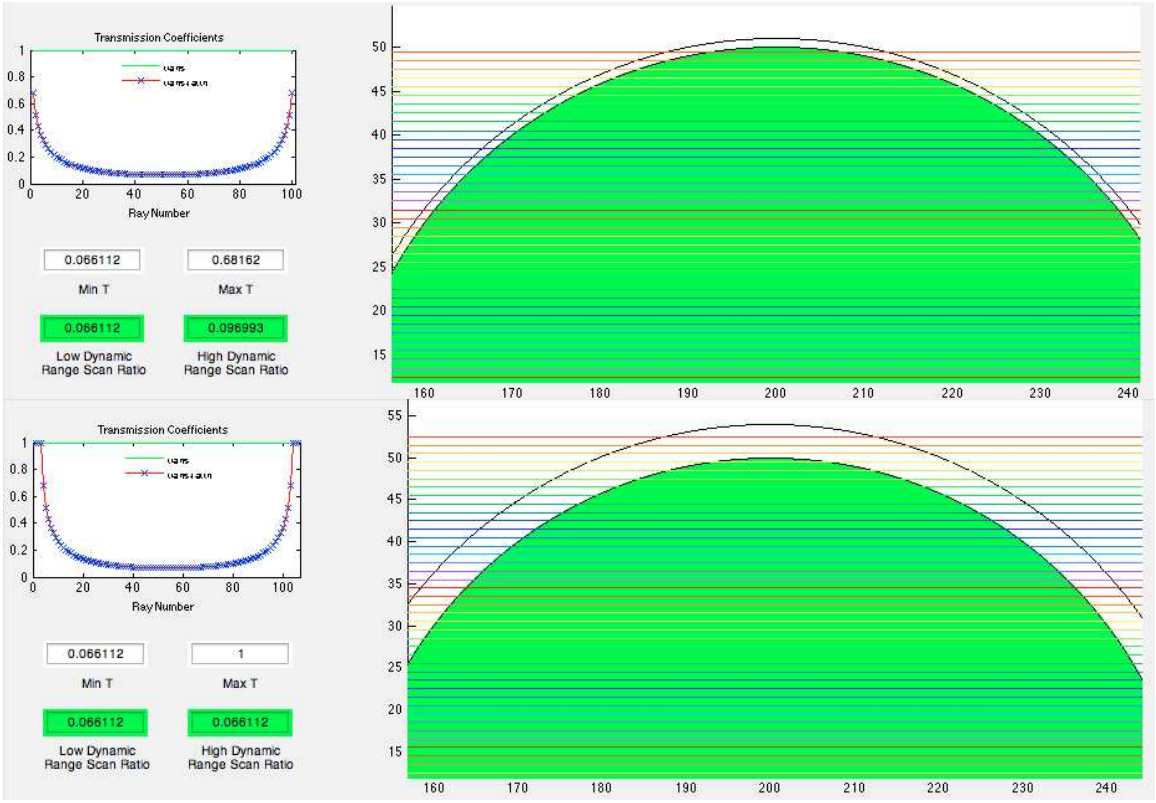

Figure 28: Increasing gap size causes decreased measurements in the usable radius for perfectly matched media due to simulation error. Top image: fluid, solid-tank, and dosimeter RI = 1.5, gap size = 1mm. Bottom image: fluid, solid-tank, and dosimeter RI = 1.5, gap size = 4 mm. As the gap size increases, more rays pass through the gap instead of the dosimeter, causing a decrease in the measured usable radius.

Figures (29)-(33) demonstrate typical results for a telecentric system, discussed in detail in Sections 3.2.1 and 3.2.2. Ray tracings are provided for perfect media matching and dosimeter-tank mismatches both with and without optimal fluid matching. Additional ray tracings are provided to show the effect of an increase in gap size for previously optimized media, then the required increase in fluid RI required to achieve optimal media matching with the larger gap size.

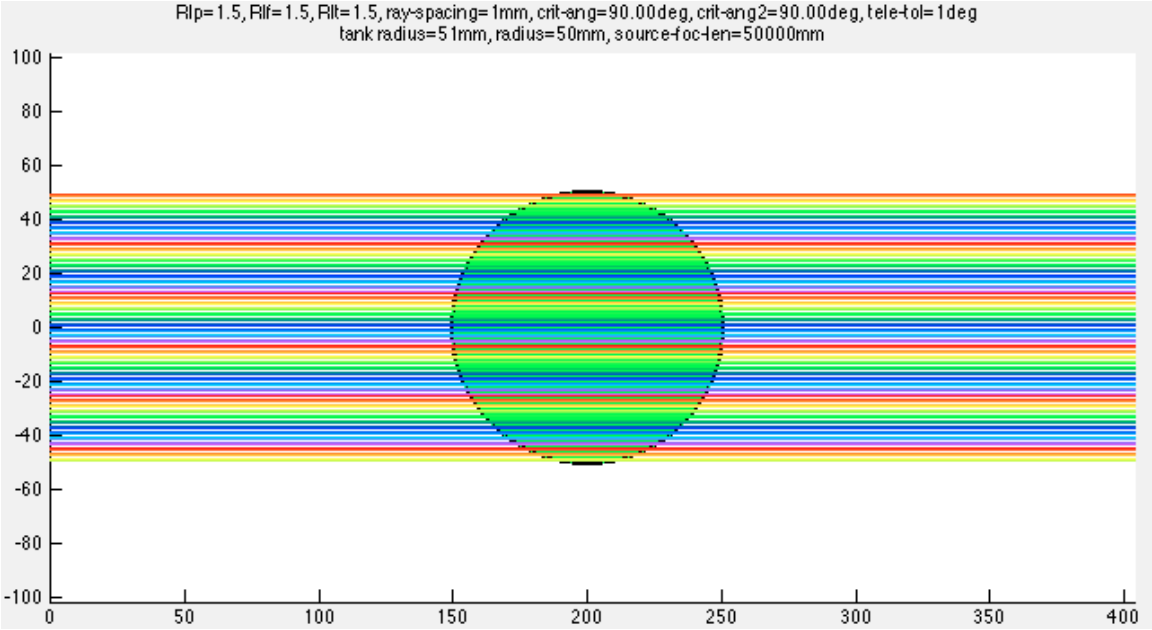

Figure 29: Perfect media matching in a telecentric system. Fluid, solid-tank, and dosimeter RI = 1.5, gap size = 1mm, lens tolerance = 1.0°. As expected, all rays meet the telecentric lens tolerance.

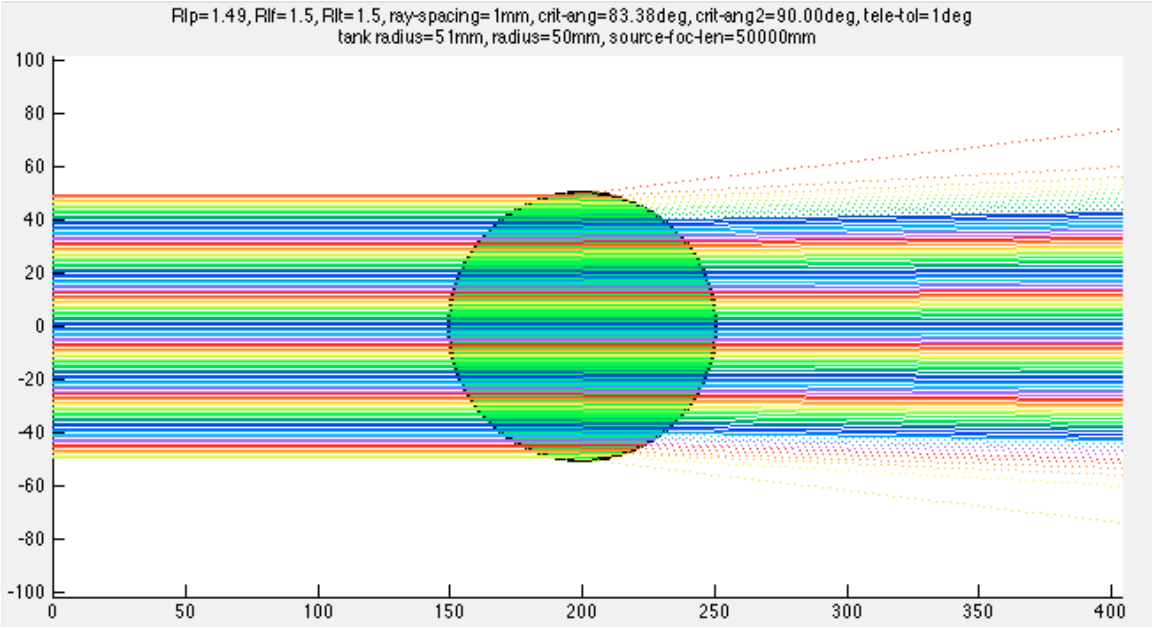

Figure 30: Dosimeter-tank RI mismatch in a telecentric system. Fluid and solid-tank RI = 1.5, dosimeter RI = 1.49, gap size = 1mm, lens tolerance = 1.0°. Compared to Figure 29, now several rays near the edge of the dosimeter are being rejected by the telecentric lens.

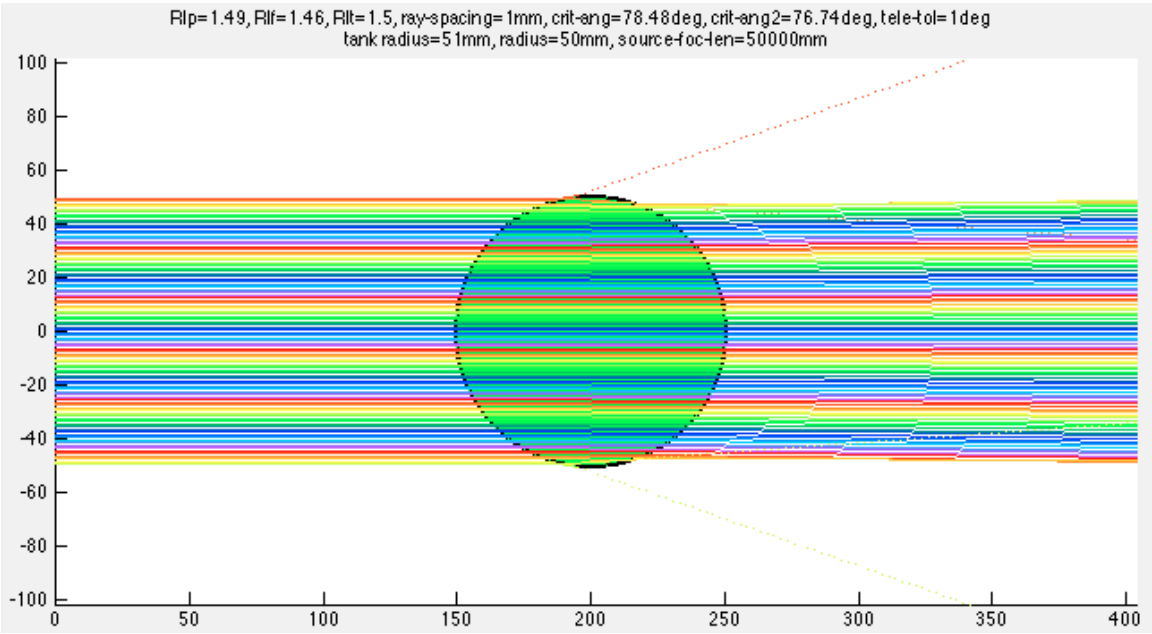

Figure 31: Dosimeter-tank mismatch in a telecentric system with optimal media matching. Solid-tank RI = 1.5, dosimeter RI = 1.49, fluid RI = 1.46, gap size =

1mm, lens tolerance = 1.0°. Because the fluid RI has been lowered to the optimal value, more rays are accepted (increasing the usable radius) compared to Figure 30.

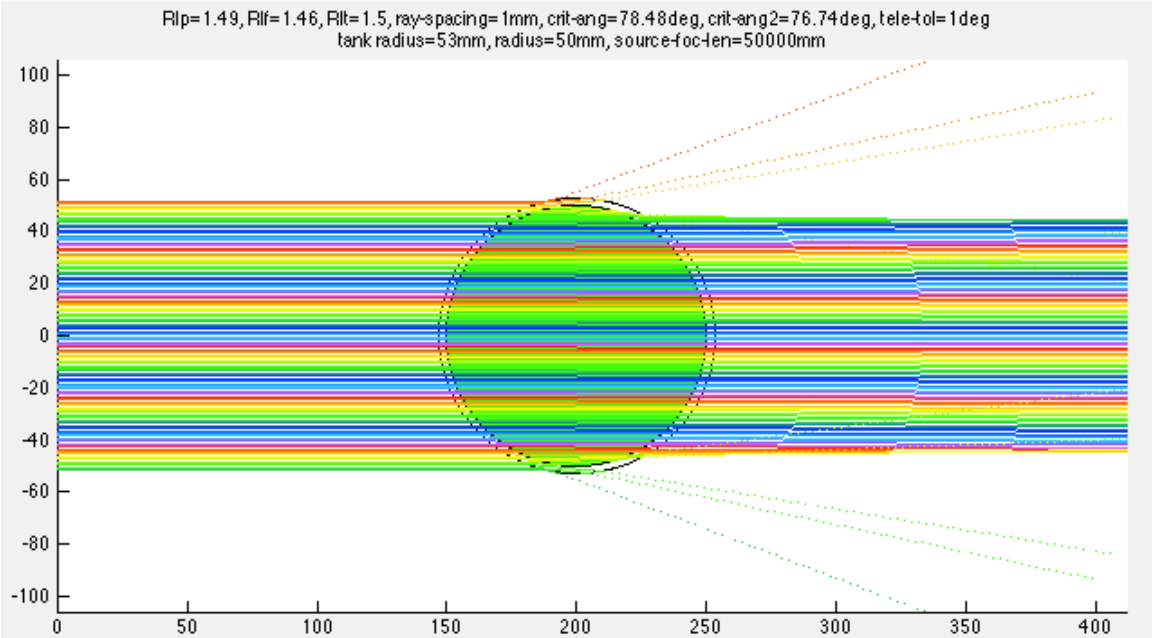

Figure 32: Increasing the gap size for the same (previously optimal) media combinations as in Figure 31 causes a decrease in the usable radius. Solid-tank RI = 1.5, dosimeter RI = 1.49, fluid RI = 1.46, gap size = 3mm, lens tolerance = 1.0°.

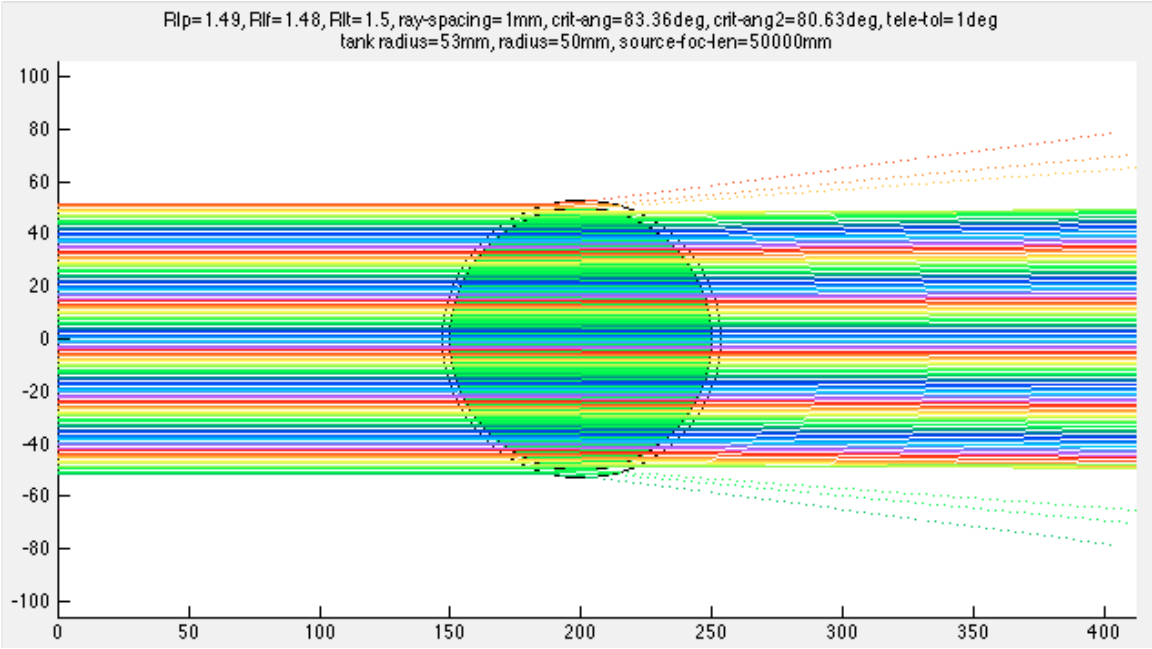

Figure 33: Optimal media matching for gap size and dosimeter-tank combination from Figure 32. With a larger gap size, the fluid RI must be raised to achieve optimal media matching and recover the usable radius. Solid-tank RI = 1.5, dosimeter RI = 1.49, fluid RI = 1.48, gap size = 3mm, lens tolerance = 1.0°.

References

1. J. Adamovics and M. J. Maryanski, Journal of Physics: Conference Series **3** (2004).

2. J. Conklin, R. Deshpande, J. Battista and K. Jordan, Journal of Physics: Conference Series **56** (2006).

3. S. J. Doran, K. K. Koerkamp, M. A. Bero, P. Jenneson, E. J. Morton and W. B. Gilboy, Physics in Medicine and Biology **46** (12) (2001).

4. S. J. Doran, Journal of Physics: Conference Series **164** (2009).

5. S. J. Doran and D. N. Yatigammana, Phys Med Biol **57** (3), 665-683 (2012).

6. J. C. Gore, M. Ranade, M. J. Maryanski and R. J. Schulz, Physics in Medicine and Biology **41** (12) (1996).

7. P. Guo, J. Adamovics and M. Oldham, Medical Physics **33** (10), 3962-3972 (2006).

8. P. Y. Guo, J. A. Adamovics and M. Oldham, Medical Physics **33** (5), 1338-1345 (2006).

9. K. T. Islam, J. F. Dempsey, M. K. Ranade, M. J. Maryanski and D. A. Low, Med Phys **30** (8), 2159-2168 (2003).

10. T. Juang, J. Newton, M. Niebank, R. Benning, J. Adamovics and M. Oldham, Journal of Physics: Conference Series **444** (2013).

11. M. J. Maryanski and M. K. Ranade, SPIE Proceedings **4320**, 764-774 (2001).

12. M. Oldham, Journal of Physics: Conference Series **56**, 58-71 (2006).

13. M. Oldham, Journal of Physics: Conference Series **250** (2010).

14. A. E. Papadakis, G. Zacharakis, T. G. Maris, J. Ripoll and J. Damilakis, IEEE Trans Med Imaging **29** (5), 1204-1212 (2010).

15. D. Ramm, T. P. Rutten, J. Shepherd and E. Bezak, Phys Med Biol **57** (12), 3853-3868 (2012).

16. D. Ramm, Journal of Physics: Conference Series **444** (2013).

17. L. Rankine and M. Oldham, Medical Physics **40** (5), - (2013).

18. H. S. Sakhalkar and M. Oldham, Medical Physics **35** (1), 101-111 (2008).

19. H. S. Sakhalkar, J. Adamovics, G. Ibbott and M. Oldham, Med Phys **36** (1), 71-82 (2009).

20. A. Thomas, J. Newton, J. Adamovics and M. Oldham, Medical Physics **38** (8), 4846-4857 (2011).

21. C.-S. Wuu and Y. Xu, Medical Physics **33** (5), 1412-1419 (2006).